15 Spectroscopic methods applied to zircon

Lutz Nasdala

Institut für Geowissenschaften – Mineralogie
Johannes Gutenberg-Universität Mainz
D-55099 Mainz, Germany

Ming Zhang

Department of Earth Sciences, University of Cambridge
Downing Street, Cambridge CB2 3EQ, United Kingdom

Ulf Kempe

Institut für Mineralogie
Technische Universität Bergakademie Freiberg
Brennhausgasse 14, D-09596 Freiberg, Germany

Gérard Panczer

Laboratoire de Physico-Chimie des matériaux Luminescents, UMR 5620 CNRS
Université Claude Bernard – Lyon 1
69622 Villeurbanne, France

Michael Gaft

International Technologies Laser
Rishon-Lezion 75140, Israel

Michael Andrut

Institut für Mineralogie und Kristallographie
Universität Wien – Geozentrum
A-1090 Wien, Austria

Michael Plötze

Institut für Geotechnik
Eidgenössische Technische Hochschule Zürich
CH-8093 Zürich, Switzerland

INTRODUCTION

Natural and synthetic (pure and doped) zircon ($ZrSiO_4$) have been studied with a variety of spectroscopic techniques. These techniques are based on different physical phenomena, for instance transitions between spin states of nuclei and electrons, energetic transitions of valence electrons, intra-molecular vibrations, or vibrations of atoms and molecular units in the lattice. All of the diverse spectroscopic techniques, however, have in common that they probe energy differences between a ground and excited states, mostly upon interaction of the mineral with incident radiation. Such interactions are not only determined by the excited elementary particles or molecules themselves but depend greatly on their local environments (i.e. number, type, valence and geometrical arrangement of neighboring atoms). Spectroscopic techniques are thus sensitive to the local structure and provide information on the short-range order.

Most research on zircon crystals using spectroscopic techniques was done to study their "real structures," that is the characterization of deviations from "perfect" zircon. Such features include

1529-6466/03/0053-0015$05.00

the incorporation of non-formula elements, structural defects and the presence of inclusions and other impurities. Correspondingly, most of the spectroscopic investigations can be assigned to two major groups. The first group represents studies done to characterize the structural position and local environment of non-formula elements when incorporated in the zircon lattice, and accompanying effects on physical properties. The second group comprises studies subjected to the real structures of "metamict" zircon samples, i.e., changes of the zircon structure caused by the impact of self-irradiation and upon recovery from radiation damage (Ewing et al., this volume).

It is most obvious that a spectroscopic bulk or point analysis will first of all yield a spectrum (i.e. a plot of the intensity of the respective physical parameter versus wavelength, frequency or wavenumber), and this is what is used in most studies. In addition, image generation based on spectroscopic data has become an increasingly applied discipline. Natural zircon crystals are normally not homogeneous in terms of chemical and structural composition, but rather show a heterogeneous pattern, which is referred to as "internal structure." Examples include oscillatory growth zoning (e.g., Connelly 2000, Hoskin 2000), sector zoning (e.g., Vavra et al. 1999) and recrystallization patterns (e.g., Pidgeon 1992). Such internal structures of natural and synthetic zircon crystals are most easily studied in electron microprobes by backscattered electron (BSE) imaging. Among the spectroscopic techniques, cathodoluminescence (CL) imaging is most commonly used. Because there is a separate chapter on internal structures and their BSE and CL imaging (Corfu et al., this volume), we will not discuss CL imaging in great detail here. Even though other spectroscopic techniques such as confocal Raman microprobe and laser-induced luminescence analysis have only been used sparsely thus far for image formation and the study of internal structures, they have a great potential in the future.

This chapter gives an overview of the diverse applications of spectroscopic analytical techniques to the investigation and characterization of zircon. This summarizing overview makes no claim to be exhaustive. It is rather focused on the more commonly used techniques such as luminescence and vibrational spectroscopy whereas other spectroscopic methods (e.g., spin resonance, thermoluminescence, photo-electron and X-ray spectroscopy) are discussed only briefly or not at all. The goal of this chapter is to demonstrate the versatile use of spectroscopic analyses and the wealth of obtained information, underlining that modern spectroscopic methods are by far more than just complementary techniques to X-ray diffraction and chemical analysis.

LUMINESCENCE SPECTROSCOPY OF ZIRCON

Cathodoluminescence of zircon

Introductory remarks. Over the last decades, CL imaging of polished grains has become a routinely used technique for the study of internal structures of zircon crystals (e.g., Sommerauer 1976, Hoffman and Long 1984, Marshall 1988, Vavra 1990, Halden and Hawthorne 1993, Koschek 1993, Hanchar and Miller 1993, Vavra 1994, Hanchar and Rudnick 1995, Hoskin 2000). Introduction of CL technique as a standard method in zircon studies was especially stimulated by the use of the U-Pb isotope system of this mineral in geochronological research (e.g., Gebauer 1990, Roger et al. 1995, Vavra et al. 1996, 1999; Whitehouse et al. 1999, Connelly 2000, Poller 2000, Rubatto and Gebauer 2000, Hermann et al. 2001). Currently, most common CL technique is panchromatic (integral) imaging using a CL detector attached to a scanning electron microscope (SEM-CL). Cathodoluminescence imaging by the aid of an optical CL microscope (OM-CL) or a combination of both methods are applied more sparsely, but until the event of modern SEM-based systems, OM-CL was the standard way of doing CL microscopy. The one primary advantage of using an OM-CL based system is that color variations in minerals can be easily seen with the unaided eye, and any photographs taken (using film or digitally) can be corrected for color accuracy (Hanchar and Rudnik 1995, Götze 1998, Götze et al. 1999, Kempe et al. 1999). Even though quite a number of studies were addressed to the study of causes of the CL emission (Sommerauer 1976, Hoffman

and Long 1984, Lork and Koschek 1991, Ohnenstetter et al. 1991, Yang et al. 1992, Remond et al. 1992, Hanchar and Rudnick 1995, Phillips et al. 1996, Kempe et al. 2000, Rubatto and Gebauer 2000, Remond et al. 2000, Poller et al. 2001), there is still controversy about the nature of the CL signal and factors influencing the CL intensity in panchromatic SEM-CL images of natural zircon crystals. However, sound understanding of the CL mechanisms is fundamental for correct interpretation of the CL intensity. In the following, we give a critical overview of the current state of knowledge of CL research.

Generation of cathodoluminescence in natural zircon. Cathodoluminescence emission results from the interaction of a primary electron beam with solids characterized by a band gap (semiconductors and insulators). The energies of the primary electron beam (up to >20 keV) and of backscattered electrons are well above the excitation energies of the CL, which are on the order of several eV. However, primary and backscattered electrons may transfer most of their energy to the lattice in the form of heat (temperatures as high as 600-700°C may be reached), characteristic and continuum X-rays, Auger electrons etc. (cf. Goldstein et al. 1981), and generate secondary electrons. These secondary electrons are characterized by a continuous energy spectrum just in the range of the excitation levels of the CL emission. The secondary electrons thus cause CL activation, provided the emission is not suppressed by quenching mechanisms (see below). In the simplest case, bonding electrons from the valence band may be excited to the conduction band and released to the ground state under emission of photons (see intrinsic luminescence in Fig. 1). The width of the band gap (i.e. the energy difference between valence and conduction bands; cf. Fig. 1) is characteristic of the investigated material and the related emission for zircon lies in the ultraviolet (UV) range around 230-280 nm (Votyakov et al. 1986, Krasnobayev et al. 1988, Cesbron et al. 1993). However, energy relaxation (the return of the excited electron to its ground level) is also possible via other radiative or non-radiative transitions involving local defects. Moreover, some centers may be directly excited (i.e. not involving band transitions or other defects) and with relaxation mecha-

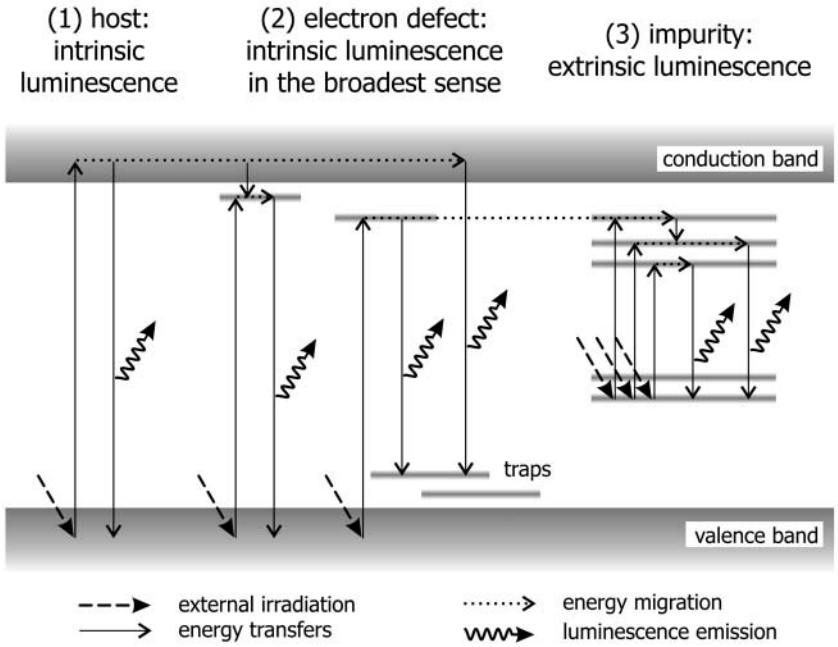

Figure 1. Simplified energy diagram showing the three principal types of luminescence generation upon electron beam irradiation. Cathodoluminescence emission may be caused by (1) band-band transitions, (2) band, trap, and electron-defect assisted transitions and (3) impurity state transitions within forbidden band gaps.

nisms that are hardly influenced by the local crystal field, as may often be found for trivalent rare earth element (REE) centers. For further details on the basic physics of CL see Marshall (1988), Remond et al. (1992, 2000), Blanc et al. (2000), and Townsend and Rowlands (2000).

Information from spectral CL studies (emission wavelength, peak width, and lifetime of the excited state) can be used to identify the emission centers. However, CL activation by the electron beam is not selective. Combination of CL studies with other techniques such as photoluminescence (PL), X-ray absorption fine structure (XAFS), or electron paramagnetic resonance (EPR) is mandatory for sound interpretation but systematic investigations on natural zircon are still scarce.

Cathodoluminescence spectra of natural zircon are complex, as they consist of different types of simultaneously emitted bands. A glance at the published data suggests that in many cases, CL is dominated by broad-band emissions (e.g., Marshall 1988, Ohnenstetter et al. 1991, Lork and Koschek 1991, Yang et al. 1992, Remond et al. 1992, Cesbron et al. 1993, Hanchar and Rudnick 1995, Götze et al. 1999, Kempe et al. 1999, 2000, Remond et al. 2000, Poller et al. 2001). For example, intrinsic luminescence and CL emission via electron defect centers localized on oxygen-bearing anion groups ($[SiO_4]^{n-}$ in zircon) appear as broad bands in CL spectra. However, CL spectra of natural zircon samples may also show a predominance or important role of narrow emission bands (Hanchar and Rudnick 1995, Götze et al. 1999, Kempe et al. 1999, Remond et al. 2000; see Figs. 2 and 3). Narrow line groups often centered at 480 and 575 nm and weaker emissions centered at 666 and 755 nm are assigned to Dy^{3+} impurities (e.g., Marshall 1988, Ohnenstetter et al.

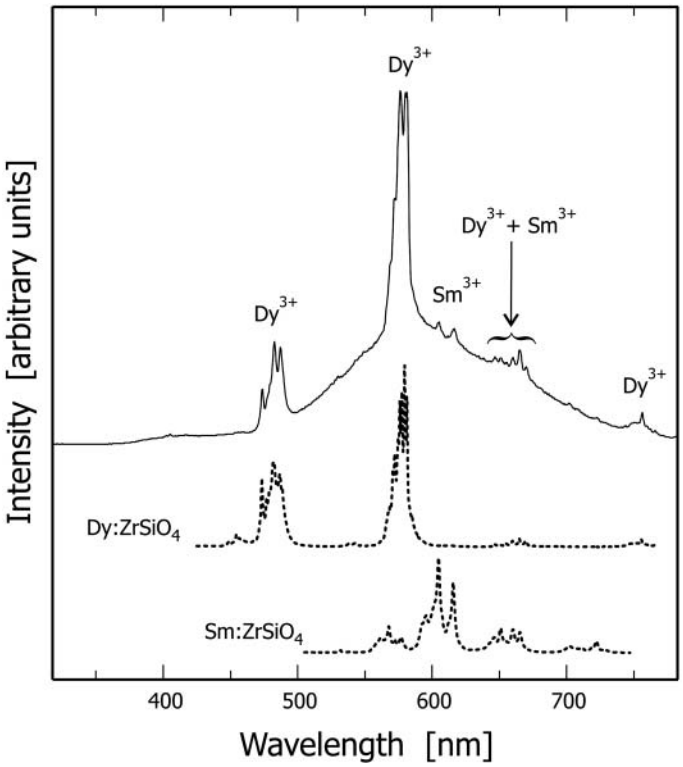

Figure 2. Cathodoluminescence spectrum (solid) of a zircon from the Cretaceous quartz sand deposit of Weferlingen, Germany (after Götze et al. 1999, redrawn and modified). The spectrum shows groups of narrow emission bands of rare earth elements, superimposed on a "yellow" broad-band emission in the range 500-700 nm. The assignment of the Dy^{3+} and Sm^{3+} band groups is underlined by comparison of this spectrum with two CL spectra (dotted) of synthetic, REE+P-doped zircon crystals (JM Hanchar, unpublished).

1991, Yang et al. 1992, Remond et al. 1992, Hanchar and Rudnick 1995, Götze et al. 1999, Kempe et al. 2000, Remond et al. 2000). This interpretation is supported by the investigation of synthetic zircon doped with Dy^{3+} (Fig. 2; cf. Cesbron et al. 1993, Blanc et al. 2000). More rarely, emission lines of other REE centers such as Er^{3+} (at 475 and 530 nm, Remond et al. 1992, 2000), Sm^{3+} (at 605 and 702 nm, Götze et al. 1999, see Fig. 2), Tb^{3+} (at 548 nm, Yang et al. 1992, Hanchar and Rudnick 1995, Nasdala et al. 2002a), Gd^{3+} (at 313 nm, Nasdala et al. 2002a) and Nd^{3+} (emission at 885 nm, Götze et al. 1999) were reported. Analogous to Dy^{3+}, the interpretation for the Er^{3+}, Sm^{3+}, Tb^{3+}, Gd^{3+}, and Nd^{3+} centers is verified by the comparison with spectra of synthetic samples (Blanc et al. 2000, see examples in Fig. 2).

Our understanding of the broad-band emissions of zircon is still poor. In accordance with the prevailing type of broad-band emission in the blue or yellow region of the spectra, Ohnenstetter et al. (1991) and Remond et al. (1992) distinguished blue and yellow luminescent zircon. There are contradictory results of spectroscopic investigations on the "blue" band emission discussed in more detail elsewhere (Kempe et al. 2000). It must, however, be mentioned that the intensity maximum of the "blue" emission lies in the UV range between 200-400 nm where most CL systems show a dramatic decrease in sensitivity, also known as quantum efficiency, or spectral response, and the spectral response of the detector used should be taken into account when quantifying CL spectra. Several spectra published in the literature suggest that "blue" zircon CL is caused by a broad band centered near 365 nm (Iacconi et al. 1980, Krasnobayev et al. 1988, Remond et al. 1992, Yang et al. 1992, Cesbron et al. 1993, Poller et al. 2001, Nasdala et al. 2002a). Iacconi et al. (1980) suggested that the "blue" luminescence of zircon is analogous to the "blue" luminescence of other silicates and can be explained by emission from electron defects localized at SiO_4 groups (cf. also Yang et al. 1992, Kempe et al. 2000). Electron defects are formed under irradiation and released electrons are trapped, for example, on a Si site ($Si^{4+} + e^- \rightarrow Si^{3+}$). Electron defects may also be stabilized by impurities such as Dy^{3+} (Krasnobayev et al. 1988, Gaft 1992, Claridge et al. 2000a). For instance, the emission band at 385 nm, observed in CL (Yang et al. 1992) as well as in thermoluminescence (TL) spectra (Kirsh and Townsend 1987, Laruhin et al. 2002) of natural zircon seems to involve both [SiO_4]-related centers and REE ions.

The "yellow" broad-band emission is often centered at 560 nm (Fig. 3D). The nature of this emission is also explained by contradictory models (e.g., Gaft 1992, Kempe et al. 2000). Possible models suggest additional electron defects on the SiO_4 tetrahedron, for example stabilized by Zr vacancies (Claridge et al. 2000), or emission from Yb^{2+} impurities (Kempe et al. 2000). However, all authors agree that the "yellow" emission center is of radiogenic origin, i.e. it is only generated in solids that were affected by radioactive irradiation (Gaft 1992, Remond et al. 1992, 2000; Kempe et al. 2000).

Factors leading to variations in the cathodoluminescence intensity. Potential causes of intensity variations of the observed CL signal include CL quenching and various effects of the crystallinity. The emission of CL may be quenched by optical absorption processes. Furthermore, there is a drastic decrease of the defect-related CL efficiency at elevated temperatures. However, even at constant temperature, the intensity of a certain REE^{3+} emission is not simply a linear function of the total content of the respective REE. The concentration of a luminescent center may deviate from the respective total element content if there are variations in the valence state. Further, interaction between neighboring emission centers of the same type may lead to energy migration and CL quenching (self-quenching or concentration-quenching) at higher concentration levels. Moreover, interaction between centers belonging to different types is also possible. In these cases, the energy may be transferred to other CL active emission centers or to centers with non-radiative relaxation (quenching centers). In both cases, however, the CL of the REE^{3+} center under consideration is quenched. By contrast, the CL emission from a REE^{3+} center may also be enhanced by energy transfer from other centers (sensitizing). To give an example, self-quenching of Dy^{3+} starts at around 1 atm % Dy according to Iacconi and Caruba (1980). The same authors found that Dy^{3+}

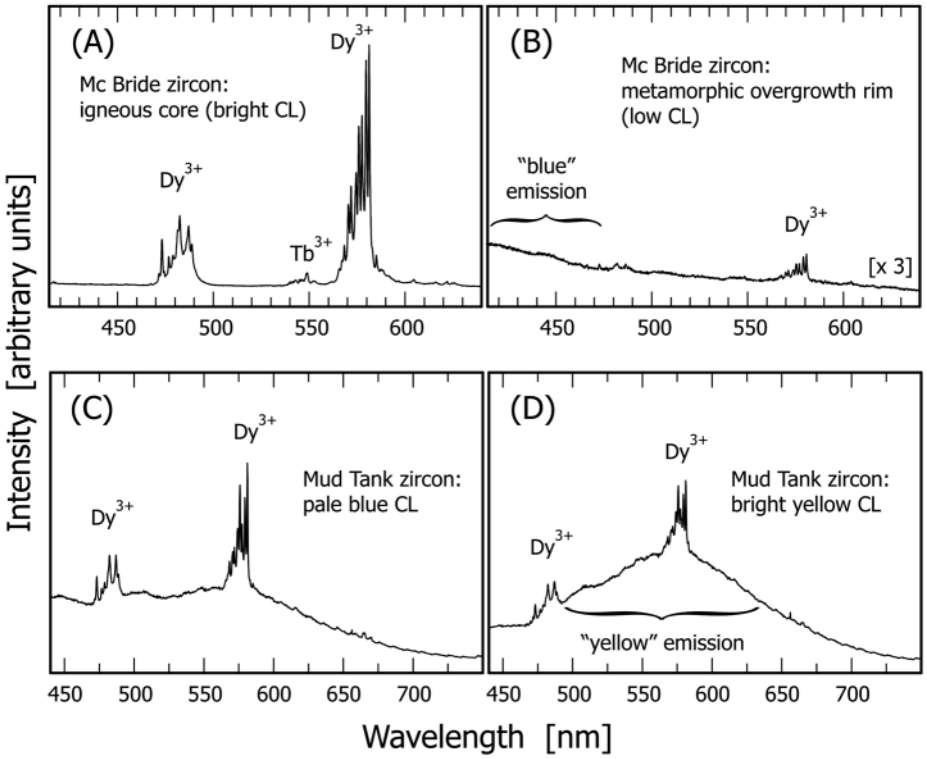

Figure 3. Complex contribution of broad-band and narrow-band emissions on the total CL signal. (A) Cathodoluminescence spectrum of an igneous core in a zircon from a xenolith, McBride province, Queensland, Australia. (B) Corresponding spectrum (intensity 3× expanded) of a metamorphic overgrowth rim in the same crystal as in A, showing very low CL intensity. Spectra modified after Hanchar and Rudnick (1995). Bright CL observed from the igneous core is due to strong REE emission bands. (C) Cathodoluminescence spectrum from a micro-area that appeared bluish in the CL microscope. Zoned zircon crystal from the Mud Tank carbonatite, Northern Territory, Australia. (D) Corresponding spectrum (same intensity scale) obtained from a yellow CL area in the same crystal as in C. Spectra from JM Hanchar and PWO Hoskin (unpublished); for sample description see Hanchar et al. (1997). The total CL emission of the blue zone appeared clearly less intense with the unaided eye, even though the Dy^{3+} emission bands are more intense. The brighter appearance of the yellow zone is due to the more intense yellow broad-band emission. All spectra were taken from areas 10 × 10 mm in size and are corrected for the instrument response (resolution 0.15 nm).

quenches the "blue" zircon CL starting from about 0.01 atm % Dy.

Intrinsic CL is closely related to the structural perfection of the host lattice. If the degree of crystallinity of zircon decreases, the emission of intrinsic CL decreases, too. This interrelation (Hoffman and Long 1984) was recently supported by combined SEM-CL and Raman microprobe studies (Kempe et al. 2000, Nasdala et al. 2002a). For zircon crystals that have not experienced self-irradiation and external irradiation, secondary recrystallization or hydrothermal alteration, the degree of crystallinity and related intrinsic CL intensity depend on the concentration of primary lattice defects (cf. Figs. 4E and F). Primary defects in natural zircon are often related to the incorporation of trace elements (Sommerauer 1976, Gracheva et al. 1981, Kempe et al. 2000). Note that the contents of typical trace elements in zircon, excluding Hf, are usually found to be correlated (Romans et al. 1975, Speer 1980, Hoffman and Long 1984, Bibikova et al. 1991, Benisek and Finger 1993, Hanchar and Miller 1993, Hanchar and Rudnick 1995, Rubatto and Gebauer 2000, Kempe et al. 2000). Thermal recrystallization, as for instance under high temperature metamorphic condi-

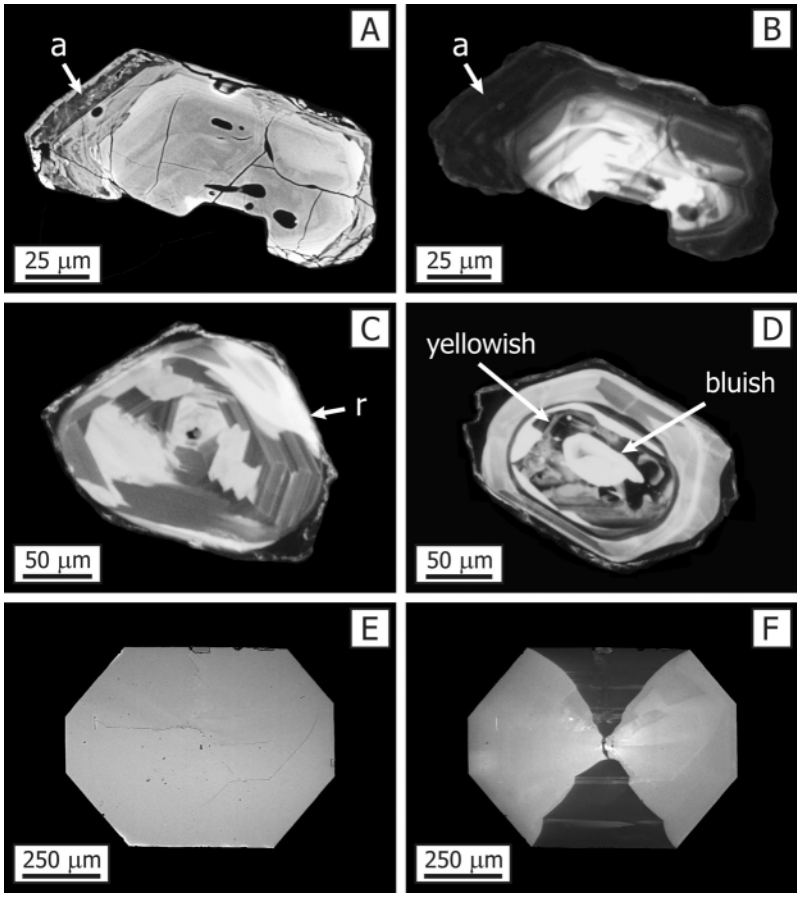

Figure 4. Images of zircon crystals obtained in a SEM (A-D, U Kempe, unpublished; E-F, A Kronz, unpublished). (A) Zircon grain with a hydrothermally altered rim (marked a) from the Eibenstock granite, Blauenthal, German Erzgebirge (BSE image). (B) Panchromatic CL image of the same grain as in A, showing CL quenching in the alteration zone (a) which is enriched in U, Th, Ca, Fe and Y. (C) Panchromatic CL image of a patchily recrystallized zircon from the Saxonian Granulite Complex, Germany. The recrystallized, yellowish luminescent area (r) emits particularly intense CL. (D) Zircon from the Saxonian Granulite Complex, Germany. The panchromatic CL image was obtained with a PMT (Oxford R4) that is more sensitive the blue than in the yellow region of the electromagnetic spectrum. As an analytical artifact, the CL intensity of a bluish luminescent core in a yellowish luminescent zircon is apparently overestimated. (E) Pure, synthetic $ZrSiO_4$ crystal, grown using the Li-Mo flux technique (Hanchar et al. 2001), BSE image. (F) Cathodoluminescence image of the crystal shown in E, revealing clear sector zoning that cannot be seen in the BSE mode. The CL emission is probably related to defects, pointing to local differences in the primary crystallinity.

tions, may improve the crystallinity of zircon through recovery from radiation damage and loss of trace elements. Correspondingly, thermally recrystallized zircon grains often show relatively high CL intensity (Fig. 4C, cf. Gebauer 1990, Vavra et al. 1999, Kempe et al. 2000, Rubatto and Gebauer 2000, Geisler et al. 2001a). By contrast, hydrothermal alteration processes may often decrease the degree of crystallinity and CL intensity. Altered areas with quenched CL are often enriched in Fe, Y, P, Ca, and U (Fig. 4A-B, Kempe et al. 2000). No correlation has been found between CL intensity and Hf content in zircon, and based on the electronic configuration of the Hf atom, it seems unlikely that Hf would contribute to the CL emission of natural zircon.

Uranium and thorium impurities have rather indirect effects on the zircon CL. Poller (2000)

and Poller et al. (2000, 2001) proposed that "U (and Hf) plays an important role in quenching the CL". This hypothesis was disproved by results of heating experiments (Geisler et al. 2001a, Nasdala et al. 2002a). After being annealed, zircon crystals were found to show strongly enhanced CL intensity even though the U (and Hf) content remained the same. Therefore, it was concluded in these studies that the mere presence of U does not quench the CL but rather the CL emission is greatly suppressed by radiation effects. The radioactive decay of trace actinides (U and Th) and their unstable daughter nuclei damages the zircon structure (Ewing et al., this volume). This radiation damage, in turn, leads to a drastic decrease of the CL intensity, particularly of the broad-band emissions. Note that even though most of the structural damage of natural zircon crystals is due to their self-irradiation, other factors such as primary lattice defects and distortions need also be considered when discussing the correlation between CL intensity and structural damage (cf. Figs. 4E and 4F). Also, the influence of Th on the structural damage and, with that, on the CL was considered insignificant in some of the earlier CL studies. However, this is only true for zircon with low Th/U ratio. In rare cases, high Th/U ratios well above one, then often accompanied by Th concentrations in the 10^3 ppm range, were found. Examples are zircon crystals from Tsakhir, Mongolian Altai, showing no SEM-CL (Kempe et al., unpublished) and primarily zoned (i.e. not recrystallized) patches in zircon grains from the Jack Hills, Western Australia (Nasdala et al. 1996), which also show extremely low CL emission (Kempe et al. 2000).

Another important effect which may be caused by self-irradiation as well as external irradiation is charge transfer (exchange of electrons and holes between neighboring centers) modifying the defect structure of the crystal. This process is well documented for natural fluorite (Chatagnon et al. 1982, Kempe et al. 2002). Similar processes are also of relevance for natural zircon (Solntsev and Shcherbakova 1973, Iacconi and Caruba 1980, Iacconi et al. 1980, Krasnobayev et al. 1988, Claridge et al. 2000). Radiation-induced charge conversion (changes in the valence state of impurity ions) produces additional electron defects that enhance broad-band CL. Charge transfer processes induced by irradiation in more or less well-crystallized zircon grains may be inverted at relatively low temperatures. "Blue" zircon CL anneals at lower temperatures than "yellow" CL because the "yellow" trap lies deeper in the band gap. However, detailed investigations on this subject are still needed.

Instrumental factors. The CL intensity in panchromatic images may be modified by the detection system used. As an analytical artifact, systems with high sensitivity in the blue region yield enhanced intensities for bluish luminescent zircon whereas the "blue" broad-band luminescence is suppressed in images obtained with detectors having low sensitivity in this wavelength range (Fig. 4D; cf. Kempe et al. 2000). Note that intensity relations between different bands and lines observed in a given CL spectrum depend also on the detection mode, i.e., parallel measurement with a multichannel detector [e.g., charge-coupled device (CCD) detector, or diode array detector] or serial data collection with a photomultiplier (PMT). In a similar manner, the presence of narrow Dy^{3+} lines is visible in CL color images as a greenish tint even when broad-band emission prevails (e.g., Götze et al. 1999, Kempe et al. 1999). By contrast, Dy^{3+} lines have only in rare cases (cf. Figs. 3A and B) a notable influence on the intensity patterns in panchromatic SEM-CL images, which is due to their low impact on the integral CL intensity (Kempe et al. 2000). Monochromatic CL imaging, however, makes it possible to trace the distribution of individual emission centers throughout a crystal. Using this technique, it has been shown that the spatial distribution of luminescent REE^{3+} impurities and electron-defect related emission centers may be quite different in one and the same crystal (Remond et al. 2000, Kempe et al. 2000).

It is essential for the correct interpretation of zircon CL images and spectra to estimate the escape depth of the CL signal. Several experiments have shown that escape depths of zircon CL are significantly larger than that of secondary and backscattered electrons. A possible explanation refers to a high efficiency of carrier diffusion with an escape of the electrons and holes away from the excitation site and following recombination for the band-related CL (Kempe et al. 2000, Norman 2002). Possible three-dimensional effects should, therefore, be considered in interpreting zircon CL

images and spectra (Kempe et al. 2000).

Although CL imaging of natural zircon is widely used in geosciences and has been the subject of quite a number of studies, some of the observed phenomena still cannot be explained in a fully convincing way by the existing theories on the CL intensity. This situation means that a simple relationship between the content of one or two trace elements in natural zircon and the panchromatic CL intensity (e.g., Vavra 1990, Poller et al. 2001) cannot be expected. Natural zircon crystals are virtually multi-doped systems and CL emission may be affected by the degree of crystallinity, the electronic structure, self- and external irradiation and the thermal history of the sample.

Laser-induced time-resolved photoluminescence of zircon

Introduction: Steady-state and time-resolved luminescence. Conventionally used steady-state or continuous-wave (CW) luminescence is a process where the excitation sources pump the sample at constant intensity over time necessary to perform the measurement. The final result is, analogous to the CL discussed above, an emission spectrum. The specificity of the technique can be improved by employing a tunable laser as the active component of the system. In an ideal system the exciting wavelength would be tunable through the large fraction of the ultraviolet and visible region of the electromagnetic spectrum. Such a system would enable one to study both the excitation and emission behavior of luminescence centers.

In spite of the great progress that has been achieved in the study of steady-state luminescence of minerals, a great number of the observed luminescence phenomena in minerals are not yet well understood. The reason is that minerals are co-doped, multi-ion compounds and the steady-state spectroscopy may be inadequate as the discriminatory power of the normal emission spectra is somewhat limited. Therefore, we need to assume that the majority of luminescence spectra published thus far is likely to consist of overlaps of several types of emissions. There is, however, another physical parameter that may be extremely useful, namely, the fluorescence lifetime or decay time. This is the exponential decay time for the fluorescence emission assuming pulse excitation. The decay time is a measure of the transition probability from the emitting level. Luminescence can be observed over time range of femto- to milliseconds. Decay time is a characteristic and unique property and no two luminescence emissions will have exactly the same decay time. The enormous dynamic temporal time range combined with intrinsic sensitivity makes time-resolved luminescence a uniquely powerful spectroscopic tool.

Both the spectral and temporal nature of the luminescence emission bands can be determined by means of time-resolved spectroscopy. By using such techniques, it is possible to separate overlapping emissions that have different origins and, therefore, different luminescence lifetimes. For this, the intensity in a specific time "window" at a given delay after the excitation pulse is recorded, where both delay and gate width have to be carefully chosen. The added value of the method is the energetic selectivity of a laser beam, which enables one to combine time-resolved spectroscopy with monochromatic excitation. Time-resolved luminescence thus provides numerous ways to detect the presence of luminescence centers (transition elements, lanthanides and actinides) in natural zircon, which would have been obscured by strong broad-band emissions under continuous excitation (steady state laser or electronic excitations).

Intrinsic broad-band photoluminescence. The PL spectrum of zircon (i.e. light emission excited by light) is similarly complex in nature as the CL discussed above. Apart from impurity-related emissions, which will be discussed below, the PL spectrum of natural zircon is often characterized by a broad intrinsic band (Taraschan 1978, Shinno 1986, Krasnobayev et al.1988, Votyakov et al. 1993, Gorobets and Rogozin 2001) in the yellow range of the electromagnetic spectrum (Fig. 5). The excitation of this emission band peaks at 310 nm (i.e., this yellow PL is most intense with 310 nm excitation). The broad yellow band at 575 nm has a decay time of 25-35 μs. It was also observed as a result of n-irradiation and α-irradiation of synthetic, initially non-luminescent $ZrSiO_4$, with the

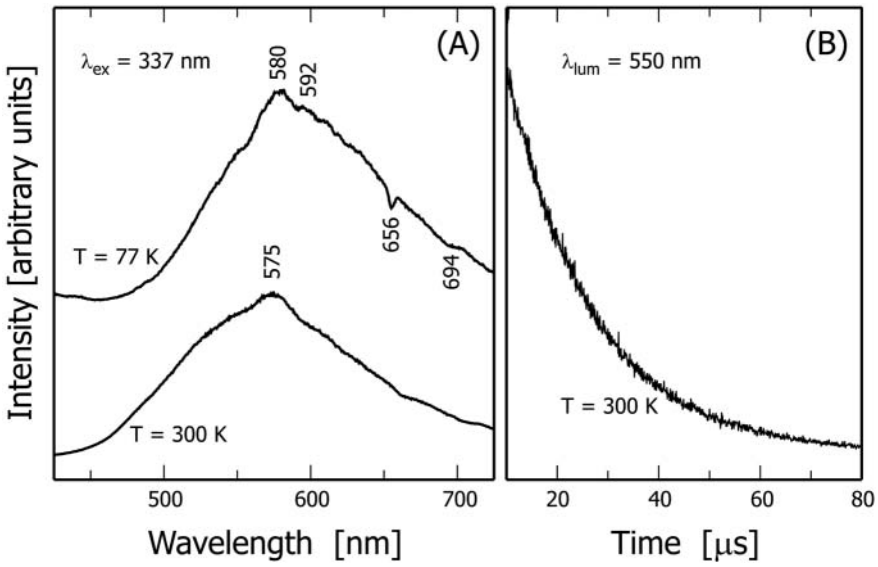

Figure 5. Intrinsic broad-band PL, which was observed from all investigated natural zircon samples thus far. (A) Spectra obtained at 300 and 77 K (spectral resolution ~1 nm). The two "negative" lines are caused by impurity U^{4+}, through reabsorption of light. (B) Decay of the yellow broad-band PL. Note that the decay of the emission intensity was not measured at the band maximum but at the high frequency slope of the band (550 nm). This was done to avoid any biased results that could potentially be caused by effects of the Dy^{3+} emission peaking at 575 nm. Redrawn (modified) from Gaft et al. (2002).

band intensity increasing proportionally with the irradiation time (Gaft et al. 2002). Analyses at 300 and 77 K with different laser excitations, delays and gates showed that, in spite of the very broad half-width and the apparently asymmetric shape, this luminescence consists of only one band. Gaft et al. (2002) found that for both alpha and neutron irradiation, such induced luminescence is stable for at least several years after irradiation. The spectral shape of this radiation-induced luminescence is very close to those of natural zircon samples. Its decay time is of approximately 30-35 μs and the intensity remains stable after heat-treatment up to 700°C, which is also characteristic for natural zircon. Gaft et al. (2002) therefore concluded that the "classical" yellow luminescence band of natural zircon (λ_{max} = 575 nm; half-width Δ = 160 nm; decay time τ = 25-35 μs), is connected with radiation-induced centers. In minerals, the source of irradiation may be connected with radioactive decay of U and Th impurities. The exact type of the yellow luminescence center needs clarification.

Impurity-related photoluminescence. Impurity-related centers in zircon may give rise to broad-band and narrow-band PL emissions. Only a brief overview is given in the following. For more details on impurity-related PL see, for instance, Taraschan (1978), Shinno (1987), Krasnobayev et al.(1988), Votyakov et al.(1993), Gaft et al.(2000b) and Gorobets and Rogozin (2001). Zircon crystals containing uranium show often intense, green luminescence that is assigned to $(UO_2)^{2+}$ centers (Fig. 6). This luminescence was also observed in synthetic zircon doped with U and P. By contrast, in synthetic zircon crystals doped either with Th and P or U only, such luminescence was not obtained. The causal connection of this emission with uranium is underlined by the fact that its intensity correlates with the U content determined by ICP-MS. Another typical luminescence feature of many natural zircon samples is a broad, deep red luminescence band (Fig. 6). This red emission is connected with forbidden d-d transitions in Fe^{3+}. It is thermally stable and dominates in zircon samples that were heat-treated at 800°C. The decay time of 1-2 ms is very long and, correspondingly, the red Fe^{3+} emission appears especially intense in spectra with long delay times in which the stronger yellow luminescence is already quenched. Strong luminescence of $Cr^{3+}$and

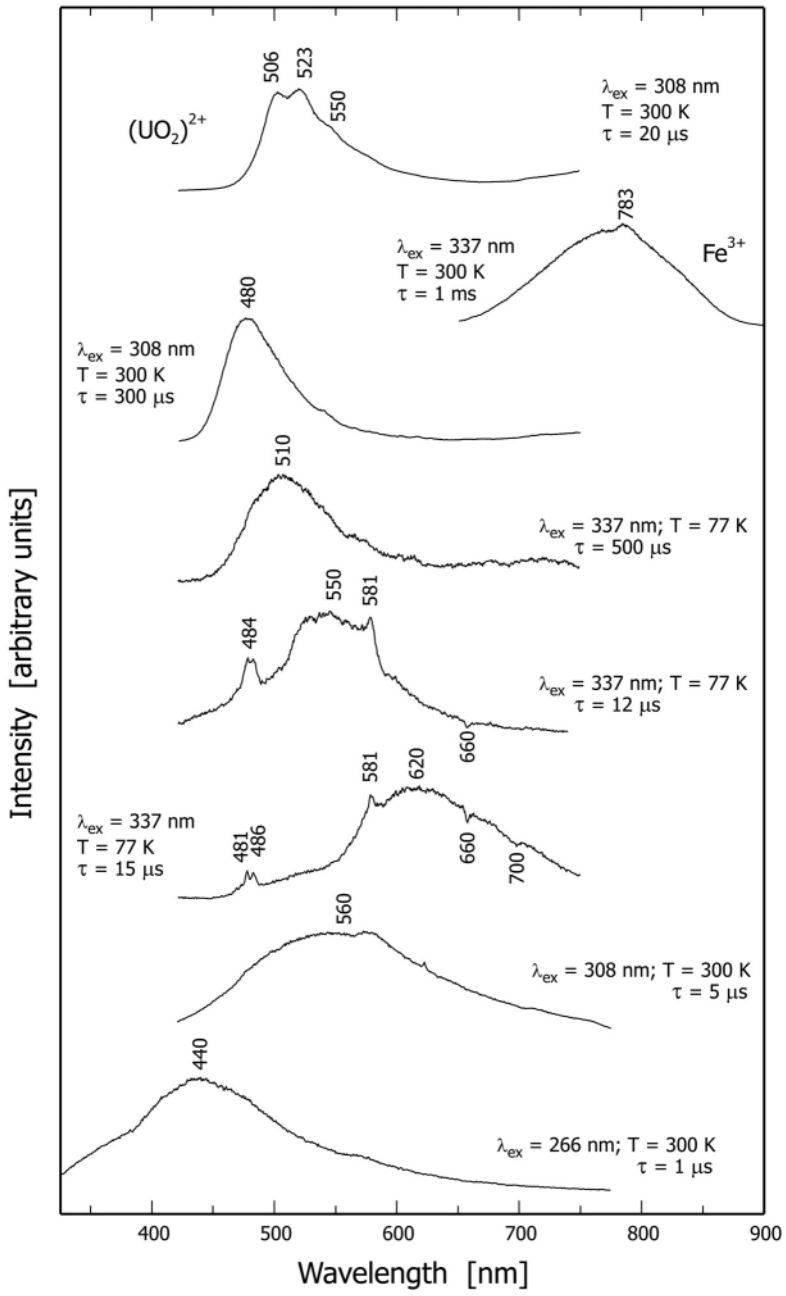

Figure 6. Impurity broad-band PL in natural zircon samples (delay time 10 ns, gate 19 ms, spectral resolution ~1 nm). Excitation wavelength, temperature and decay time (τ) are individually reported for each spectrum. The two upper spectra are assigned to $(UO_2)^{2+}$ and Fe^{3+}, respectively. The other six spectra show emissions of unidentified centers. As in Figure 5, "negative" reabsorption lines in the range 650-700 nm are due to traces of U^{4+}. Spectra: G Panczer and M Gaft (unpublished).

Cr^{5+} in the red and IR parts of the electromagnetic spectrum has been observed from synthetic, doped $ZrSiO_4$ but not for natural zircon thus far. Finally, REE^{3+} centers, which give rise to mostly narrow-band emissions, are particularly typical of zircon. There are several REE impurities that are not detectable or difficult to detect under UV excitation but easily revealed by laser-induced

Table 1. Examples for characteristic emission lines and decay times of chromium and rare-earth elements in natural zircon. Data after Gaft et al. (2000a,b,c; 2001).

Center	λ_{lum} [nm]	λ_{ex} [nm]	t [µs]	Transition
Cr^{3+}	694	532	3-5	$^2E \rightarrow {}^4A_2$ (R-lines),
	775		3-5	$^4T_2 \rightarrow {}^4A_2$ (broad)
Cr^{5+} (300 K)	1213	532	2×10^{-1}	$^2E \rightarrow {}^2T_2$
Cr^{5+} (12 K)	1132	532, 1060	2×10^{-2}	$^2E \rightarrow {}^2T_2, {}^2B_1 \rightarrow {}^2A_1$
	1154			
	1191			
	1215			
	1258			
Ce^{3+}	355	266	2×10^{-2}	$^2D \rightarrow {}^2F$
Pr^{3+}	489	337	1	$^3P_0 \rightarrow {}^3H_4$
	596		10	$^1D_2 \rightarrow {}^3H_4$
	621		10	$^1D_2 \rightarrow {}^3H_4$
Sm^{3+}	565	337	550	$^4G_{5/2} \rightarrow {}^6H_{5/2}$
	601, 612		550	$^4G_{5/2} \rightarrow {}^6H_{7/2}$
	647		550	$^4G_{5/2} \rightarrow {}^6H_{9/2}$
Eu^{3+}	596	337	1500	$^5D_0 \rightarrow {}^7F_1$
	616		50	$^5D_0 \rightarrow {}^7F_2$
	654		1500	$^5D_0 \rightarrow {}^7F_3$
	702		1500	$^5D_0 \rightarrow {}^7F_4$
	707		1500	$^5D_0 \rightarrow {}^7F_4$
Gd^{3+}	312	266	2500	$^6P \rightarrow {}^8S_{7/2}$
Tb^{3+}	383	266	325	$^5D_3 \rightarrow {}^7F_6$
	415		325	$^5D_3 \rightarrow {}^7F_5$
	437		325	$^5D_3 \rightarrow {}^7F_4$
	489		2400	$^5D_4 \rightarrow {}^7F_6$
	548		2400	$^5D_4 \rightarrow {}^7F_5$
Dy^{3+}	478	337	120	$^4F_{9/2} \rightarrow {}^6H_{15/2}$
	575		120	$^4F_{9/2} \rightarrow {}^6H_{13/2}$
Ho^{3+}	549	337	1	$^5S_2 \rightarrow {}^5I_8$
	665		1	$^5F_3 \rightarrow {}^5I_7$
Er^{3+}	549	337	10	$^4S_{3/2} \rightarrow {}^4I_{15/2}$
	559		10	$^4S_{3/2} \rightarrow {}^4I_{15/2}$
Tm^{3+}	289	266	15	$^1I_6 \rightarrow {}^3H_4$
	347		15	$^1I_6 \rightarrow {}^3H_6$
	458		5	$^1D_2 \rightarrow {}^3H_4$
	483		120	$^1G_4 \rightarrow {}^3H_6$

or/and time-resolved luminescence spectroscopy. The characteristics of REE^{3+} emission lines identified for zircon are given in Table 1 and selected spectra are presented in Figure 7.

In addition, a number of unidentified luminescence bands (Fig. 6) were observed from natural zircon samples. These are usually obscured by stronger emissions and may be detected only by time-resolved spectroscopy. These bands are most probably related to impurities. To identify the exact nature of these impurities, synthetic $ZrSiO_4$ doped with potential activators such as Mn, Cr, Ti, Co, Ni, Pb and Sb have been studied (Gaft et al. 2002). Bands similar to those detected in natural zircon, however, were not observed from the synthetic samples. The nature of the corresponding luminescence centers needs further investigation.

The emission of PL does not only depend on the luminescent center itself but is also affected by crystal field effects (cf. Marfunin 1979a,b), particularly in radiation-damaged zircon. Because it is known that the yellow PL of natural zircon is partially radiation-induced, nominally pure zircon irradiated by different doses of X-ray, γ-ray, neutron and α-irradiation have been studied (Gaft et al. 2002). Table 2 presents the comparison of the half width of the Dy^{3+} main emission line obtained from different natural and synthetic samples. Note that its FWHM (full width at half band-maximum) shows clear correlation with the degree of crystallinity. Another example is presented in Figure 8, which shows the broadening of several REE^{3+} emissions (see in particular the two $^4G_{5/2} \rightarrow {}^6H_{7/2}$ transitions of Sm^{3+} at 604 and 615 nm). Photoluminescence and especially time-resolved PL thus allows one to estimate the concentration of irradiation-induced defects via the intensity of the broad defect emission or via the width of the rare earth emission lines.

VIBRATIONAL SPECTROSCOPY OF ZIRCON

Infrared absorption spectroscopy of zircon

Assignment of infrared absorption bands. For the tetragonal $ZrSiO_4$ ($I4_1/amd$), seven infrared-active modes (internal = $2A_{2u} + 2E_u$, external = $A_{2u} + 2E_u$) are predicted by group theory (Dawson et al. 1971). According to the selection rules, modes of E_u symmetry are observed when the electric vector of the incident infrared radiation, ***E***, is perpendicular to the c-axis while those of A_{2u} symmetry are observed when ***E*** is parallel to the *c*-axis. Polarized infrared (IR) measurements were carried out to identify the E_u and A_{2u} modes and to obtain the transverse optical (TO) and longitudinal optical (LO) modes (Dawson et al. 1971, Gervais et al. 1973, Zhang and Salje 2001). Frequencies of the main infrared-active TO and LO modes, their damping and band assignments are compiled in Table 3. Among the four internal SiO_4 vibrations, two are assigned to

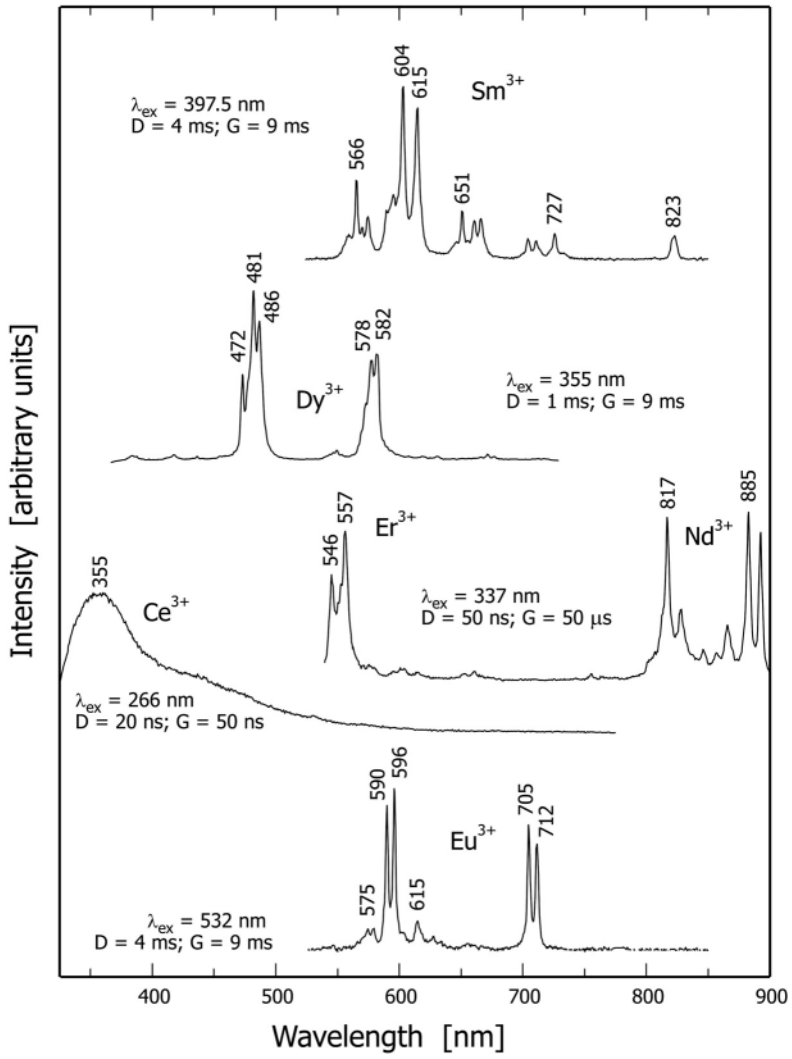

Figure 7. Examples for time-resolved spectra of emission lines of rare-earth elements in zircon (spectral resolution ~1 nm). Excitation wavelength, delay (D) and gate (G) are given for each individual spectrum. Spectra: G Panczer and M Gaft (unpublished).

Table 2. Effects of the crystallinity of zircon on the half-width of the 581 nm Dy^{3+} emission line ($^4F_{9/2} \rightarrow {}^6H_{13/2}$). Data after Panczer (2001).

Sample	Band half-width [nm]
Synthetic, Dy^{3+}-doped zircon	0.57
Natural zircon, non-metamict	0.76
Natural zircon, metamict (untreated)	2.10
Natural zircon, metamict (heat-treated at 800°C)	0.72

Table 3. Infrared-active TO and LO modes of crystalline zircon. Data after Zhang and Salje (2001).

E_u ($\boldsymbol{E} \perp$ c)					A_{2u} ($\boldsymbol{E} \parallel$ c)				
w_{TO}	G_{TO}	w_{LO}	G_{LO}	assignment	w_{TO}	G_{TO}	w_{LO}	G_{LO}	assignment
282	7	351	7	external (R)	338	10	475	12	external (T)
385	9	416	7	external (T)	606	9	644	17	$\nu_4(SiO_4)$
431	5	470	3	$\nu_4(SiO_4)$	980	13	1101	15	$\nu_3(SiO_4)$
880	11	1030	12	$\nu_3(SiO_4)$					

All values (frequency w and damping G) are given in cm^{-1}.
R = rotary vibration, T = translatory vibration.

$\nu_3(SiO_4)$ (anti-symmetric stretching, A_{2u} at 980 cm^{-1} and E_u at 880 cm^{-1}) and the other two are assigned to $\nu_4(SiO_4)$ (anti-symmetric bending, A_{2u} at 606 cm^{-1} and E_u at 431 cm^{-1}), whereas the $\nu_1(SiO_4)$ and $\nu_2(SiO_4)$ modes (symmetric stretching and bending vibrations of the tetrahedrons, respectively) are not infrared active due to symmetry reason. By contrast, Kolesov et al. (2001) listed the A_{2u} mode near 980 cm^{-1} as $\nu_1(SiO_4)$. The assignment of the three external modes (two translatory and one rotary) in the far-infrared, which are mainly related to SiO_4 group motions against Zr atoms and motions of Zr atoms (Farmer 1974), is still controversial. Dawson et al. (1971) and Kolesov et al. (2001) assigned the E_u mode near 385 cm^{-1} mainly as a rotary vibration of the SiO_4 tetrahedrons and the E_u mode near 282 cm^{-1} as a translatory mode, whereas Farmer (1974) and Zhang et al. (2001) attributed the former as translatory mode and the latter as rotary vibration.

An advantage of the infrared spectroscopy is that the absorption of infrared light is mainly dependent on atomic masses and the length and strength of interatomic bonds. Therefore, infrared spectra can give valuable information on the crystal structure, composition and surface of the studied material. Due to its short length scale it probes, infrared spectroscopy may reveal local structural configuration of crystalline and amorphous phases. In addition, using polarized incident radiation, one can obtain information of anisotropy and anharmonicity, and determine dielectric constants as well as TO and LO phonon bands from infrared reflection spectroscopy.

The effect of cation substitutions and chemical impurities on IR band frequencies of zircon

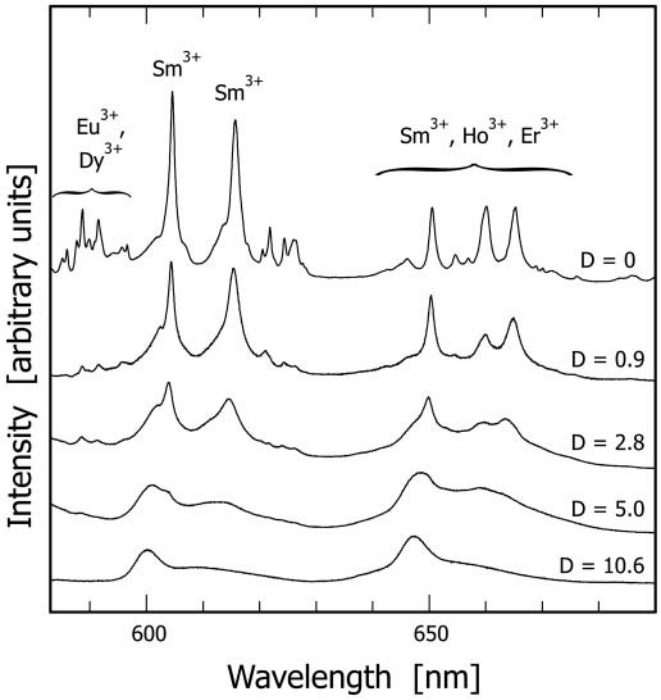

Figure 8. Effects of radiation damage in zircon crystals from Sri Lanka on their laser-induced PL spectra, here shown for the red region of the electromagnetic spectrum. Spectra (488 nm excitation, resolution 0.1 nm) were modified from Nasdala et al. (submitted) and are stacked for more clarity. With increasing radiation damage, REE^{3+} emission lines are broadened. To provide a measure for the increasing metamictization, radiation doses (D) are given in 10^{18} α-events per gram. These values represent the total time-integrated self-irradiation lasting for a ~550-570 Myr period (the U-Pb zircon age). Note that the Sri Lankan zircon crystals have experienced partial structural reconstitution (e.g., Nasdala et al. 2001d). The presently observed radiation damage is, therefore, significantly lowered and does not correspond with the calculated α-doses anymore. To provide comparability with the literature, however, total α-doses are given in this and the following figures.

and structural analogues has been the subject of several spectroscopic investigations. Hubin and Tarte (1971) studied the relationship between the frequencies of the stretching and bending bands of the SiO_4 and GeO_4 groups and ionic radius of tetravalent Zr, U, Th, Hf, and Ce ions. These authors found that among the cations studied, the substitution of Hf^{4+} for Zr^{4+} results in a small frequency shift due to the close values of the radius, whereas substitutions of other ions with relatively large radius (e.g., U^{4+} and Th^{4+}) causes a more pronounced impact on the bands frequencies. More detailed investigations of the vibrational spectra of zircon, thorite, hafnon, coffinite and their structural analogues, as well as calculations of the constants and frequencies of the vibrations, active in IR- and Raman spectroscopy, were reported, for instance, by Caruba et al. (1975), Povarennych et al. (1977), Lazarev et al. (1980), and Heyns et al. (1990). Infrared data of synthetic hydroxylated zircon crystals (Caruba et al. 1985) showed that the incorporation of $(OH)^-$ groups in the zircon lattice results in changes of unit-cell parameters as well as frequency shifts of the main ν_3 (SiO_4) and ν_4(SiO_4) IR modes.

Effects of radiation damage on the phonon spectrum of zircon. In addition to the assignment of the infrared spectrum of crystalline zircon and the identification of this mineral using IR spectroscopy as a fingerprint technique, many of the early IR studies on zircon were subjected to radiation damage phenomena (e.g., Launer 1952, Saksena 1961, Akhmanova and Leonova 1961, 1963;

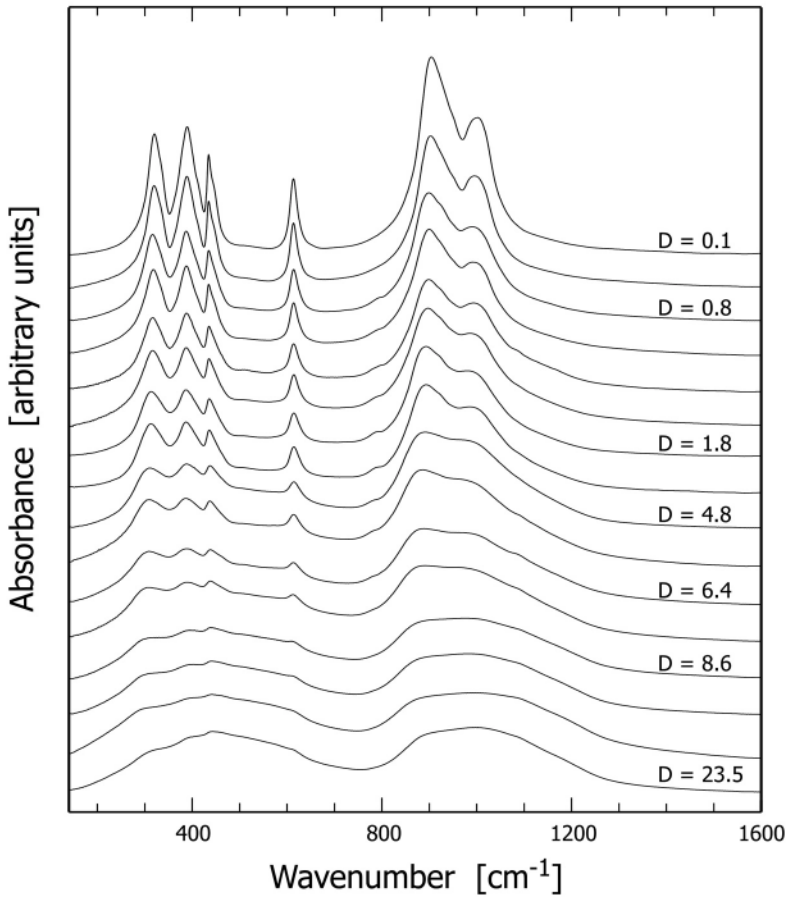

Figure 9. Radiation damage effects in zircon crystals from Sri Lanka on their infrared spectra in the range 150-1600 cm^{-1} (redrawn after Zhang and Salje 2001, modified). Absorption spectra are stacked for more clarity. Doses are given as in Figure 8.

Kristanovic 1964, Alexanian et al. 1966). Figure 9 shows the effect of α-event damage on the infrared spectrum of zircon. Different spectral parameters have been used to estimate the degree of damage or radiation dose, as for instance the width of the 616 cm^{-1} band (Deliens et al. 1977), the position and shape of the $\nu_3(SiO_4)$ band near 980 cm^{-1} (Rakovich and Gevorkyan 1988, Yang et al. 1990), the infrared reflectivity of intratetrahedral bands (Zhang and Salje 2001) and multi-phonon interactions (Wasilewski et al. 1973, Woodhead et al. 1991a, Zhang et al. 2002). Zhang and Salje (2001) demonstrated how to use the effective medium theory, an approach used to study effective dielectric and optical properties of materials with multi-phases (Granqvist and Hunderi 1978), to quantitatively analyze the fraction of the amorphous phase in metamict zircon.

Extensive IR spectroscopic investigations were stimulated by the aim to understand the real structure of metamict zircon and structural changes at the atomic level caused by the impact of radioactivity. Based on previous investigations, Pellas (1965) proposed that zircon decomposes into ZrO_2 and SiO_2 as a result of metamictization. Wasilewski et al. (1973) reported infrared data supporting the decomposition model, and these authors suggested a two-stage damage process involving the deformation of SiO_4 tetrahedrons and the sequent breakdown of the zircon lattice into the oxides. However, the model was contradictory to the results of Akhmanova and Leonova (1961) and Vance (1975) who did not detect characteristic signals of ZrO_2 and SiO_2 in untreated zircon samples. Wasilewski et al. (1973) argued that the absence of the oxides in the study of Akhmanova and Leonova (1961) could be due to incurred insufficient radiation damage. Recent spectral studies, however, did not favor ZrO_2 and SiO_2 as the final state of metamictization of zircon. Based on their mid-infrared data, Woodhead et al. (1991a) reported that the structure of metamict zircon consisted of distorted and disoriented isolated SiO_4 tetrahedrons with few if any undisplaced Zr cations. Polarized reflectance measurements (Zhang et al. 2000c) revealed that in the SiO_4 stretching region, the spectra of metamict zircon show features very different from that of glassy SiO_2. Zhang and Salje (2001) observed the change of local configurations in zircon crystals and the formation of new Si–O–Si linkages and possible partial polymerization, i.e., SiO_4 tetrahedrons may not remain fully isolated in metamict zircon. Partial polymerization in metamict zircon was also revealed by ^{29}Si nuclear magnetic resonance (NMR) measurements (Farnan and Salje 2001).

Infrared spectroscopic characterization of thermally or hydrothermally annealed zircon has resulted in new insights into the recrystallization and structural recovery of metamict zircon. The effect of high-temperature annealing on infrared spectra of metamict zircon was an increase in intensity and band sharpening. (e.g., Biagini et al. 1997). Vance (1975) showed that the decomposition of metamict zircon into ZrO_2 and SiO_2 could take place during high-temperature annealing. The recent study of Colombo et al. (1999) reported a two-stage recovery, a relaxation of the SiO_4 tetrahedrons and the possible formation of new phases. Zhang et al. (2000c) concluded from the oriented dependence of mid-infrared spectra obtained from metamict zircon that the recrystallization process in zircon involves epitaxial growth of the residual crystalline phase and reaction of ZrO_2 and SiO_2 produced by decomposition. Infrared data also showed that recrystallization of zircon is a multi-stage process and that it strongly depends on the initial degree of damage of the metamict zircon (Zhang and Salje 2002). The recrystallization process was also characterized using multi-phonon bands (Woodhead 1991a, Zhang et al. 2002). Geisler et al (2002) used the powder absorption technique to monitor the structural recovery and recrystallization in a highly metamict zircon upon hydrothermal annealing. Their data revealed spectral variations taking place at temperature as low as 200°C and the presence of monoclinic ZrO_2 at higher temperatures.

Hydrous species in zircon. Hydrous species (OH and H_2O) in zircon have been the subject of extensive infrared studies. Natural zircon containing as much as 16.6 wt % water (which is more than 50 mol %) was described by Coleman and Erd (1961). Such high water content was always related to a significantly radiation-damaged structure. By contrast, only traces of $(OH)^-$ groups are primarily incorporated in (crystalline) zircon (Woodhead et al. 1999a,b, Ilchenko and Korzhinskaya 1993, Ilchenko 1994, Nasdala et al. 2001b).

Infrared spectroscopy has been widely used to investigate hydrous species in zircon because of its high sensitivity to hydrogen-bearing substances and advantages in determination of the directions of O–H dipoles. Most infrared studies on hydrous species in zircon have been focused on the following issues: (1) the nature of hydrous species and their incorporation into the crystal lattice of zircon, (2) their possible role in metamictization, and (3) their thermal stabilities and their role in the recrystallization process.

Frondel (1953) proposed the substitution $(OH)_4 \leftrightarrow SiO_4$ in zircon. By contrast, Mumpton and Roy (1961) found that data from chemical analysis of natural zircon lie along $ZrSiO_4$-H_2O join and this was taken as evidence for the presence of molecular H_2O rather than $(OH)^-$ groups by these authors. Studies of Rudnitskaya and Lipova (1972) suggested the simultaneous occurrence of molecular water and hydroxyl groups. An infrared study of Woodhead et al. (1991b) indicated that the principal hydrous component in metamict zircon is $(OH)^-$ rather than H_2O because of the lack of the H-O-H bending mode near 1630 cm^{-1} and the combination (bending + stretching) mode at around 5200 cm^{-1}. The results from most recent spectral investigations of hydrous species in zircon are still controversial. The work of Nasdala et al. (2001b) indicated the simultaneous presence of both hydroxyl groups and molecular water in metamict zircon whereas the results of Zhang et al. (2002) essentially supported the observations of $(OH)^-$ by Woodhead et al. (1991b). Few studies to determine hydrogen locations in natural zircon have been done thus far. Woodhead et al. (1991b) suggested that the 3420 cm^{-1} ($\boldsymbol{E} \parallel c$) and 3385 cm^{-1} ($\boldsymbol{E} \perp c$) are associated with Si-occupied tetrahedrons, and weak absorption near 3510 cm^{-1} ($\boldsymbol{E} \parallel c > \boldsymbol{E} \perp c$) is attributed to OH sites at vacant tetrahedrons. Ilchenko and Korzhinskaya (1993) and Ilchenko (1994) found wide set of hydroxyl groups of different thermal stability in zircon crystals from kimberlites. Nasdala et al. (2001b) proposed three crystallographic models for probable locations of $(OH)^-$ groups in crystalline zircon. As the local structure of the metamict state of zircon is still under debate, it is currently impossible to obtain a clear picture on the hydrous sites in metamict state. The hydrous ions in amorphized materials are expected to have complex sites which produce a broad absorption between 2500 and 3600 cm^{-1}.

The possible role of hydrous components in metamictization and recrystallization in metamict minerals has drawn the attention of researchers. Figure 10 shows the effect of radiation damage on the O–H stretching bands in zircon. Studies of Frondel and Collette (1957) and Geisler et al. (2002) indicated that the presence of H_2O appears to lower the recrystallization temperature and increases the recrystallization rate of metamict zircon. By contrast, results obtained from hydrothermal experiments (Pidgeon et al. 1966, 1973) suggested that H_2O has little effect on the recrystallization rate of metamict zircon. Based on the similarities of spectral features between synthesized hydroxylated zircon and metamict zircon, Caruba et al. (1985) proposed that natural metamict zircon is formed at low temperature in a hydrous and fluorinated environment and OH is essential in metamictization process. A hypothesis that hydrous species stabilize the metamict state of zircon was proposed by Aines and Rossman (1985, 1986). By contrast, recent investigations suggested that hydrous species in metamict zircon are predominantly secondary in nature, i.e. the majority of hydrogen incorporation into metamict zircon must have occurred during or after sustaining radiation damage (Woodhead et al. 1991b, Nasdala et al. 2001b, Zhang et al. 2002). In these same studies it has also turned out that hydrogen incorporation is not necessary to stabilize the metamict state, even though hydrous species may help to compensate for local charge imbalance.

Raman spectroscopy of zircon

Introductory remarks. Infrared absorption and Stokes-type Raman scattering are similar insofar as energy of an incident beam of light is used to excite vibrations of molecular units and lattice vibrations in the analyzed sample. Quantum energies of these vibrations (phonons) correspond typically with the photon quantum energies of mid-infrared light, which is why infrared light can be absorbed upon the excitation of vibrations. Raman spectroscopy uses ultraviolet, visible or near

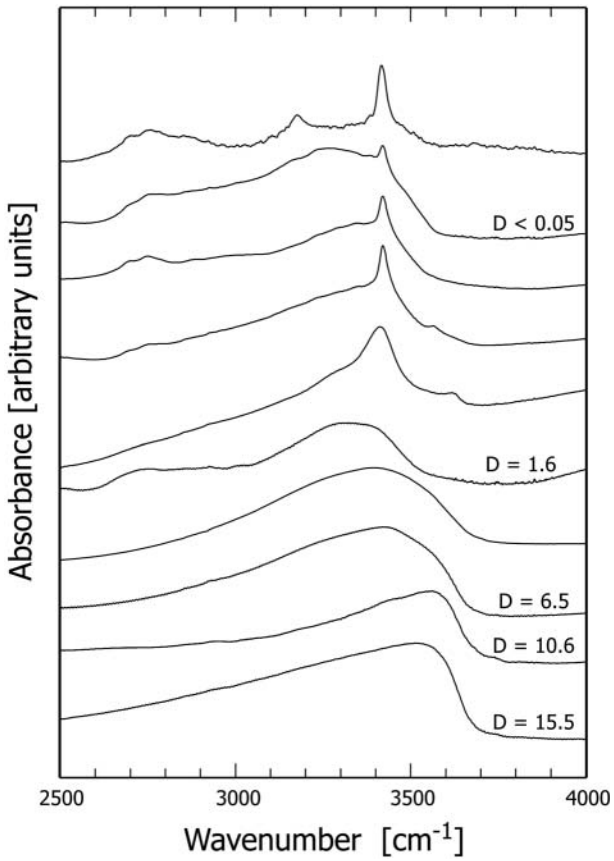

Figure 10. Polarized infrared absorption spectra (***E*** ∥ *c*) in the O–H stretching region obtained from natural zircon crystals of different origin (redrawn after Nasdala et al. 2001b, modified). Spectra are shown stacked, with increasing metamictization from top to bottom. Since samples had different thicknesses, intensities of absorption bands cannot be directly compared. Doses for five zircon samples from Sri Lanka are given as in Figure 8.

infrared light. Due to their much higher energies, such photons cannot be absorbed though the excitation of vibrations only. By contrast, if light and sample interact in a way that inelastic collisions of photons with the molecule or lattice result in the excitation of vibrations in the sample (Raman scattering), only a small portion of the photon energy is used. Correspondingly, the resulting Stokes-type Raman scattered light has lost this energy portion and is shifted towards lower wavenumbers (redshift). Analogous to the infrared absorption, the Raman effect is sensitive to the nearest environment of the vibrating bond(s). Raman spectra provide information about the local symmetry such as geometrical factors, bond force ratios and bond distances, and the short-range order of the analyzed material. For the physical background see, for example, Long (1977) and McMillan (1985).

Raman spectrum of crystalline, pure $ZrSiO_4$. The number and symmetry of Raman- and infrared active vibrations are derived through group theory and symmetry analysis (e.g., Dawson et al. 1971). From this, twelve Raman-active ($2A_{1g} + 4B_{1g} + B_{2g} + 5E_g$) in addition to seven infrared-active modes are predicted. The Raman spectrum of zircon is shown in Figure 11. It is dominated by internal vibrations of SiO_4 tetrahedrons, with the most intense band at 1008 cm^{-1} (B_{1g} mode, only observed with ***E*** _|_ c) assigned to the antisymmetric SiO_4 stretching mode. To avoid confusion of terms, it should be noted that the nomenclature for internal vibrations is inconsistently used in the literature. For example, the antisymmetric SiO_4 stretching (ν_3 internal mode) is sometimes referred

to as ν_3(Si–O) and sometimes as $\nu_3(SiO_4)$. We prefer to use the latter expression in this paper. Internal stretching and bending modes involve vibrations of all bonds of a molecular unit. The four Si–O bonds of a tetrahedron cannot vibrate independently from one another. Also, it is obvious that at least two bonds must stretch to get an antisymmetric vibration. Expressions such as ν_3(Si–O) seem, therefore, somewhat imprecise.

Even though the Raman spectra of zircon-type orthosilicate minerals are well known since the 1970s (Griffith 1970, Dawson et al. 1971, Nicola and Rutt 1974, Syme et al. 1977, Mazhenov et al. 1979), there is still some disagreement about the assignment of observed Raman bands to vibrations. The interpretation of the three main bands at 439, 974 and 1008 cm^{-1} (Fig. 11) as internal SiO_4 modes is apparently unambiguous. It is also generally agreed that the three bands at 202, 214 and 225 cm^{-1} are lattice modes (i.e. vibrations involving movements of SiO_4 tetrahedrons and Zr ions). There is, however, disagreement about the 202 cm^{-1} band which was interpreted as rotary (Nicola and Rutt 1974) and translatory vibration (Dawson et al. 1971, Syme te al. 1977, Mazhenov et al. 1979, Kolesov et al. 2001). The relatively strong band at 356 cm^{-1} band was described as external lattice mode by Syme et al. (1977) and Mazhenov et al. (1979) and as internal mode [$\nu_4(SiO_4)$, antisymmetric bending] by Dawson et al. (1971) and Ilchenko et al. (1988). The latter assignment seems problematic because the antisymmetric bending of SiO_4 tetrahedrons (ν_4), involving movements of Si^{4+} ions, is to be expected at higher frequency than their symmetric bending ν_2 at 439 cm^{-1} (analogous to the higher frequency of ν_3 when compared with ν_1, cf. Fig. 11). Correspondingly, Kolesov et al. (2001) have assigned two low-intensity bands at 641 cm^{-1} (B_{1g}) and 546 cm^{-1} (E_g) to internal $\nu_4(SiO_4)$ vibrations whereas they described the strong 356 cm^{-1} band as external mode. The assignment of the 641 cm^{-1} band to $\nu_4(SiO_4)$, however, was critically discussed by Hoskin and Rodgers (1996) who suspected this ν_4 mode might either be incorrectly assigned or mixed with an external mode. Similar disagreement exists for the band at 393 cm^{-1} band (internal, Dawson et al.

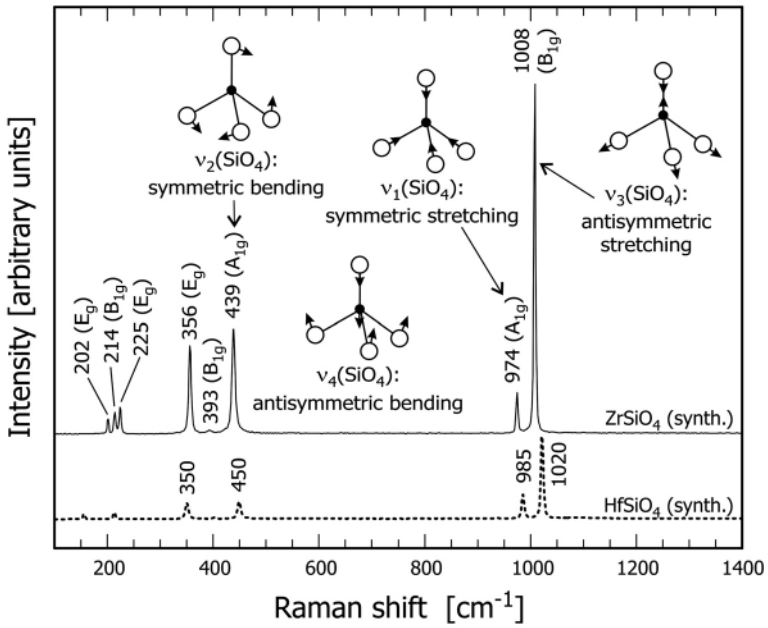

Figure 11. Raman spectrum of zircon with general band assignment for the most intense bands. For the internal SiO_4 vibrations, small sketches depict movements of oxygen (white balls) and silicon atoms (small black balls). The internal $\nu_4(SiO_4)$ vibration, the assignment of which is still controversial, is not related to a certain band in the picture. The Raman spectrum of hafnon (dotted) is shown for comparison. Note that the spectra of the two orthosilicate minerals are dominated by a greatly similar "fingerprint" pattern of SiO_4 vibrations.

1971, external, Syme et al. 1977).

In spite of these minor uncertainties about the band assignment, the Raman spectrum of zircon is highly typical of this mineral and facilitates its unambiguous identification by Raman "fingerprinting." Raman spectroscopy is also routinely applied for the identification and characterization of solid, fluid and gas inclusions in zircon. Apart from the general petrologic and mineralogical interest in inclusions, the host mineral zircon has gained particular attention for such studies. To give an example, due to its extraordinary chemical and physical stability, zircon is able to "trap" high-temperature and high-pressure phases such as microdiamonds (Nasdala and Massonne 2000) and facilitates their transportation to the Earth's surface without transformation or decomposition.

Effects of the chemical composition on the Raman spectrum. The incorporation of non-formula elements in crystalline solids causes general changes of Raman spectral parameters for both internal and external modes, which include frequency shifts, band width increase and also changes of the band shapes such as asymmetries. Depending on nature, extent and effects of the incorporation (e.g., substitution of ions in the lattice with or without major symmetry decrease, incorporation of other molecular units, formation of clusters), Raman bands of the host mineral may also split and lose intensity and additional bands may appear.

In general, effects of non-formula elements in zircon on the Raman spectrum are widely similar to changes in the infrared absorption spectrum (see above). Only a limited number of systematic investigations have been done so far to study and quantify how variations in the chemical composition affect the Raman spectrum of zircon. The substitution of Th^{4+}, U^{4+} or Hf^{4+} for $^{[8]}Zr^{4+}$ does not cause major structural changes except unit cell expansion or contraction, respectively. The pattern of Raman bands remains therefore essentially the same but vibrational frequencies shift due to slightly changed bond forces and bond angles and different cation masses. This was first observed by simply comparing the spectra of zircon with $ThSiO_4$ (Syme et al. 1977) and $HfSiO_4$ (Nicola and Rutt 1974). Raman spectral changes in the zircon-hafnon solid solution were studied in more detail by Hoskin and Rodgers (1996). A study on zircon crystals doped with Y and rare earth elements is currently in progress (Hanchar et al. in preparation). As an example, we present Raman spectra of $ZrSiO_4$ doped with Yb^{3+}+P^{5+} (Yb in the range 4-12 wt %) in Figure 12. De Waal et al. (1996) studied $ZrSiO_4$ doped with vanadium and they reported additional, low-intensity Raman bands assigned to vibrations of $(VO_4)^{4-}$ groups. These authors concluded that V^{4+} most probably occupies the $^{[4]}Si^{4+}$ site, which is in contrast to earlier results [e.g., Demiray et al. (1970) concluded from electronic absorption measurements that V^{4+} occupies the $^{[8]}Zr^{4+}$ site].

Even though a large number of non-formula elements can be incorporated by natural zircon, their concentration is mostly clearly below the 1 wt % level except for hafnium. Correspondingly, Raman spectra of most natural zircon samples show only minor effects due to their actual chemical composition. Based on the Raman data of Hoskin and Rodgers (1996) it may be concluded that even if as much as 25 % of all $^{[8]}Zr^{4+}$ ions were replaced by Hf^{4+}, frequency upshifts of the four main Raman bands (cf. Fig. 11) would not exceed 3 cm^{-1}. Spectral changes caused by the mere presence of uranium are almost negligible because of the low U^{4+} concentration in natural zircon. Nasdala et al. (2002a) found that Raman shifts and band widths obtained for a crystalline zircon containing ~ 6000 ppm U and ~16300 ppm Hf (produced through heating of a natural, metamict gemstone) deviated less than 1 cm^{-1} from data of pure $ZrSiO_4$. Also, Nasdala et al. (2001b) found that obtaining O–H stretching and particularly O–H–O bending bands from natural zircon containing hydrous species below 0.5 wt % H_2O is close to the analytical limits of current Raman systems. More pronounced Raman spectral changes are, therefore, only expected for (rare) natural zircon samples which are exceptionally rich in non-formula elements, such as in hydrothermal alteration zones (cf. Frondel 1953, Pointer et al. 1988, Rubin et al. 1989).

Effects of radiation damage on the Raman spectrum. More than 40 years ago (Launer 1952, Akhmanova and Leonova 1961, Saksena 1961) infrared studies showed that there are dramatic changes in the vibrational behavior of natural zircon in dependence on the degree of

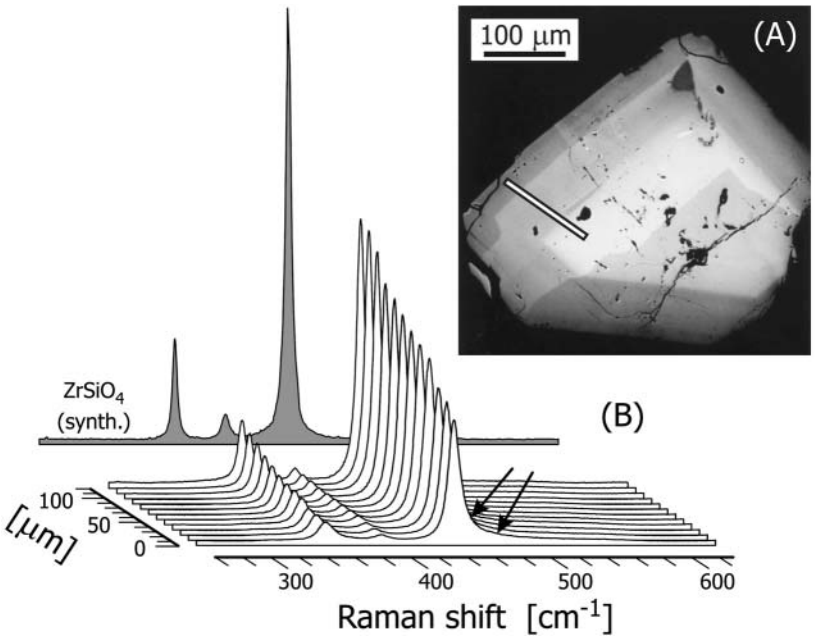

Figure 12. Example for Raman spectral changes caused by non-formula elements. (A) Backscattered electron (BSE) image of a zircon crystal doped with Yb^{3+} (4-12 wt %) and P^{5+} (for details see Hanchar et al. 2001). Bright BSE zones correspond to high dopant levels and vice versa. (B) Raman line scan, i.e., point measurements placed 11 µm apart from one another, obtained along the trace shown in A (JM Hanchar and L Nasdala, unpublished). Only a part of each Raman spectrum is shown in the plot for more clarity. The spectrum of pure $ZrSiO_4$ obtained under similar orientation (gray) is also shown for comparison (cf. also Fig. 11). With increasing Yb concentration, heights of Raman bands decrease and their widths increase. Note the clear asymmetry of the $\nu_2(SiO_4)$ band at the high-frequency side, marked with two arrows.

metamictization. In view of this, it seems surprising that no attempts were made to apply Raman spectroscopy to the study of radiation-damaged zircon until the early 1990s (Nasdala 1993, Nasdala et al. 1995). Since then, Raman spectroscopy has gained increasing attention as an undemanding but powerful technique that facilitates quantitative estimation of the degree of metamictization in zircon single crystals or micro-areas. This technique has the analytical advantages that analyses can be made without destruction of the sample, sample preparation is virtually unnecessary, and analyses can be done on a micron-scale (modern confocal Raman systems have a lateral resolution of about 1 µm and a volume resolution better than 5 μm^3, respectively). Applications were presented, for instance, by Nasdala et al. (1996), Wopenka et al. (1996), Pidgeon et al. (1998), Nasdala et al. (1998a,b; 1999), Zhang et al. (2000a,b), Balan et al. (2001), Geisler et al. (2001a,b), Högdahl et al. (2001) and Nasdala et al. (2001a,b,d; 2002a). These studies made use of the Raman spectroscopic determination of the degree of radiation damage in zircon micro-areas to constrain U-Th-Pb dating results, to estimate the ratio between α-damage retention and recovery, and to relate observed changes of chemical and physical parameters to the structural damage.

Raman spectral changes caused by radiation damage are presented in Figure 13. Causes for these spectral changes can be adequately explained only for little to moderately metamict zircon, i.e., below the first percolation point [cf. the percolation model for metamictization (Salje et al. 1999); see also Ewing et al. (this volume)]. Any interpretation needs to be cautiously done for higher degrees of radiation damage, particularly in view of the still insufficient knowledge about the real structures of strongly metamict zircon.

Raman spectra of little to moderately metamict zircon samples show the same band pattern

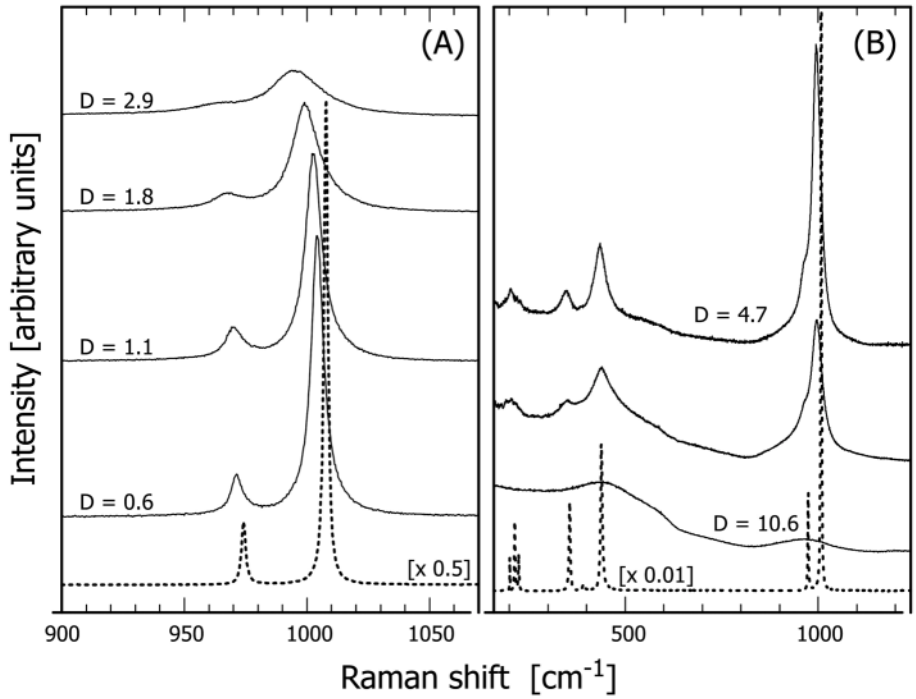

Figure 13. Effects of metamictization on the Raman spectra of zircon. (A) Four spectra in the SiO_4 stretching range obtained from little to moderately metamict, gemstone-quality zircon crystals from Sri Lanka (Nasdala et al. submitted), in comparison with non-metamict, synthetic $ZrSiO_4$ (dotted). With increasing radiation damage, Raman bands are lowered in intensity, become significantly broader and shift towards lower wavenumbers. (B) Spectra of strongly metamict zircon samples (solid, after Nasdala et al. 2002b, modified) in comparison with synthetic $ZrSiO_4$ (dotted). Note that at high damage levels, the broadened and weakened Raman signal of the remnant crystalline zircon does not have a flat background anymore but it rather overlaps with the Raman pattern of amorphous $ZrSiO_4$. The spectrum marked "D = 10.6" shows only the Raman signal of amorphous zircon. Self-irradiation doses (D) for six zircon samples from Sri Lanka age given as in Figure 8.

as crystalline zircon, however, bands are clearly broadened (decreasing short-range order) and shifted towards lower wavenumbers (structural widening). The bands are still well shaped (symmetric Gaussian-Lorentzian peaks) at this stage (see Fig. 13A). Nasdala et al. (1998a) found that the FWHM of the intense $\nu_3(SiO_4)$ mode at ~1000 cm^{-1} increases most sensitively with increasing radiation damage. This parameter was then used in most of the recent studies to estimate the degree of metamictization. The $\nu_3(SiO_4)$ broadening reflects the decreasing short range order or the increasing irregularity of SiO_4 tetrahedrons, respectively, caused by their distortion and tilting in the lattice. At advanced radiation damage [FWHM of the $\nu_3(SiO_4)$ band above 20 cm^{-1}], Raman bands of crystalline zircon continue to broaden and loose intensity and become increasingly asymmetric. The reason for the latter is still unclear. Band asymmetries (also observed in solid solutions) could, for example, point to greatly different site symmetries, partial polymerization of SiO_4 tetrahedrons (cf. Zhang and Salje 2001) but also to confinement effects [i.e. band broadening of lattice modes due to phonon lifetime decrease in very small (below 3 nm) particles]. The latter was proposed by Geisler et al. (2001b), though for zircon samples showing symmetric bands, which is most unlikely. Critical aspects of the phonon confinement hypothesis in the case of zircon will not be discussed here; the reader is referred to Nasdala et al. (2002b).

With progressive metamictization, the Raman signal of the amorphous volume fraction increases (Fig. 13B). Since crystalline zircon is a much better Raman scatterer than amorphous zircon (note the tremendous intensity loss of Raman bands upon metamictization), Raman spectra

are dominated by Raman bands of crystalline zircon even at high levels of radiation damage. To elucidate this with an example, see the upper Raman spectrum shown in Figure 13B. The amorphous fraction of this particular zircon has not been determined, however, for the Sri Lankan zircon, a total self-irradiation dose of 4.7×10^{18} α-events per gram would correspond to an amorphous volume fraction of 40 % (Holland and Gottfried 1955, X-ray diffraction) or 65-70 % [Ríos et al. 2000 (X-ray diffraction), Farnan and Salje 2001 (NMR), Zhang and Salje 2001 (infrared absorption)], respectively. In spite of the high fraction of amorphous zircon, the discussed Raman spectrum is dominated by strongly broadened bands of the remnant crystalline fraction. Note that even at elevated radiation damage, only Raman bands of (crystalline) zircon or amorphous $ZrSiO_4$ are observed, which reconfirms that self-irradiation does not cause major decomposition of zircon into oxides.

More recently, Raman spectroscopy is also applied to study the recovery of zircon from radiation damage upon annealing in the laboratory (Zhang et al. 2000b, Geisler 2001b, Nasdala 2002a,b) and natural alteration processes (Nasdala 2002b, A Willner, in preparation). All of these studies reconfirmed that structural reconstitution is not the direct inverse of progressive metamictization. For example, band broadening and frequency decrease correlate in the progressive metamictization process (Fig. 13), but this is not necessarily true anymore after the annealing treatment. Heat treatment of a moderately metamict zircon may cause marked frequency increase and only moderate FWHM decrease whereas electron beam irradiation would cause preferential FWHM decrease without major frequency change (Fig. 14B). Precise interpretation of these observations cannot be given at present. It is clear, however, that (1) the recovery strongly depends on the treatment, (2) causes of the spectral changes in radiation-damaged zircon may be heterogeneously removed during the reconstitution process, and (3) additional effects such as micro-strain and temperature-induced nucleation need to be considered. For example, as mentioned above, crystalline ZrO_2 is not formed due to self-irradiation only but is typically observed upon heat-treatment of highly metamict zircon. Therefore, even though being a most powerful tool for the study of radiation-damaged zircon and its changed chemical and physical properties, laboratory experiments are unable to retrace metamictization step by step back to undamaged zircon.

Image generation from Raman scattered light. There are two general ways to generate images from Raman data. The direct imaging technique uses the CCD detector of a Raman system like a photocamera. Such images show the intensity distribution of light of a certain (pre-set) wavelength range in the pictured area. The Raman mapping technique is greatly different. Here, a full Raman spectrum is obtained for each pixel of the map. Images age generated through processing the whole data set and may show the x-y-distribution of virtually any Raman parameter (such as band intensities, intensity ratios, background slopes, FWHMs, degrees of band asymmetry). Raman maps are typically generated from data sets containing about 10000 spectra. Advantages and disadvantages of the two techniques were compared by Lehnert (2000) and Nasdala (2002). In Figures 14 and 15, we present examples for Raman mapping. We have elucidated above that Raman spectra of natural zircon samples are closely controlled by radiation damage whereas the chemical composition has mostly only minor effects. Images generated from Raman data of natural zircon crystals thus show mainly the distribution of radiation damage. This technique opens up great opportunities for the study of internal structures. For instance, Raman images and maps combined with element maps from electron microprobe and SEM analysis may prove useful to distinguish between chemical and structural causes of intensity variations in CL images of natural zircon grains.

OTHER SPECTROSCOPIC TECHNIQUES

Electronic absorption spectroscopy

General remarks. Colors of minerals are caused by wavenumber-dependent processes in the visible part of the electromagnetic spectrum, which are studied by means of optical spectroscopy [also electronic or ultraviolet-visible-near infrared (UV-VIS-NIR) spectroscopy]. Electronic spectra

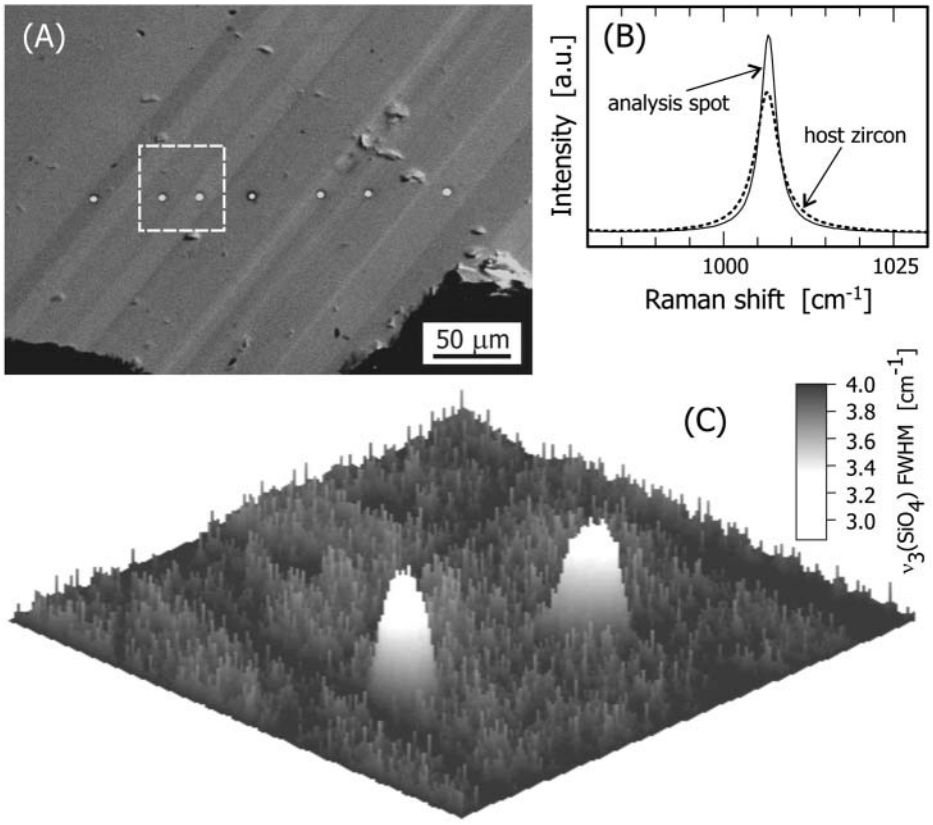

Figure 14. Local structural reconstitution of zircon caused by the impact of the electron beam during electron microprobe analysis. (A) Cathodoluminescence image of a zircon from a syenite gneiss, Renfrew County, Ontario (sample 91500, for description see Wiedenbeck et al. 1995). The locations of seven electron microprobe analyses are indicated by small bright spots. (B) Raman point analyses done in and outside the left spot in A. Structural recovery in the analysis spot areas is recognized from the FWHM decrease, which is not accompanied by notable band frequency increase in this case. (C) Raman map (area marked in A) in perspective representation, showing the lateral extension of structural effects.

are concerned with qualitative and quantitative measurements of the absorption, reflection and emission of light on powdered samples or single crystals in the spectral range 40000 to 4000 cm^{-1} (250 to 2500 nm). Absorption spectra of minerals in this energy range are affected by a number of different phenomena which are given in the following. Approximate energy ranges and the theory describing the respective process are given in squared brackets. (1) Ligand-metal charge transfer (LM-CT) [>30000 cm^{-1}, molecular orbital (MO) theory, self-consistent field X-alpha (SCF-X) procedure] describes transitions between energy states predominantly centered at the oxygen ligands of coordination polyhedra and those predominantly centered at the central ion. (2) Metal-metal charge transfer (MM-CT), [24000-9000 cm^{-1}, exchange theory] is related to electron hopping between transition metal cations in edge- or face-sharing coordination polyhedra. (3) Crystal field transitions [30000-4000 cm^{-1}, crystal field theory, superposition model (SM), angular overlap model (AOM)] include electronic transitions between crystal field split d- or f-states, localized at cations. (4) Absorption due to color centers is caused by excitations of electrons allocated at lattice defects. (5) In addition, fundamental, overtones and combination modes of groups or molecules can be found up to ~8000 cm^{-1} [vibrational theory of isolated groups].

Zircon may show a large variety of colors, depending on the content of transition metals and

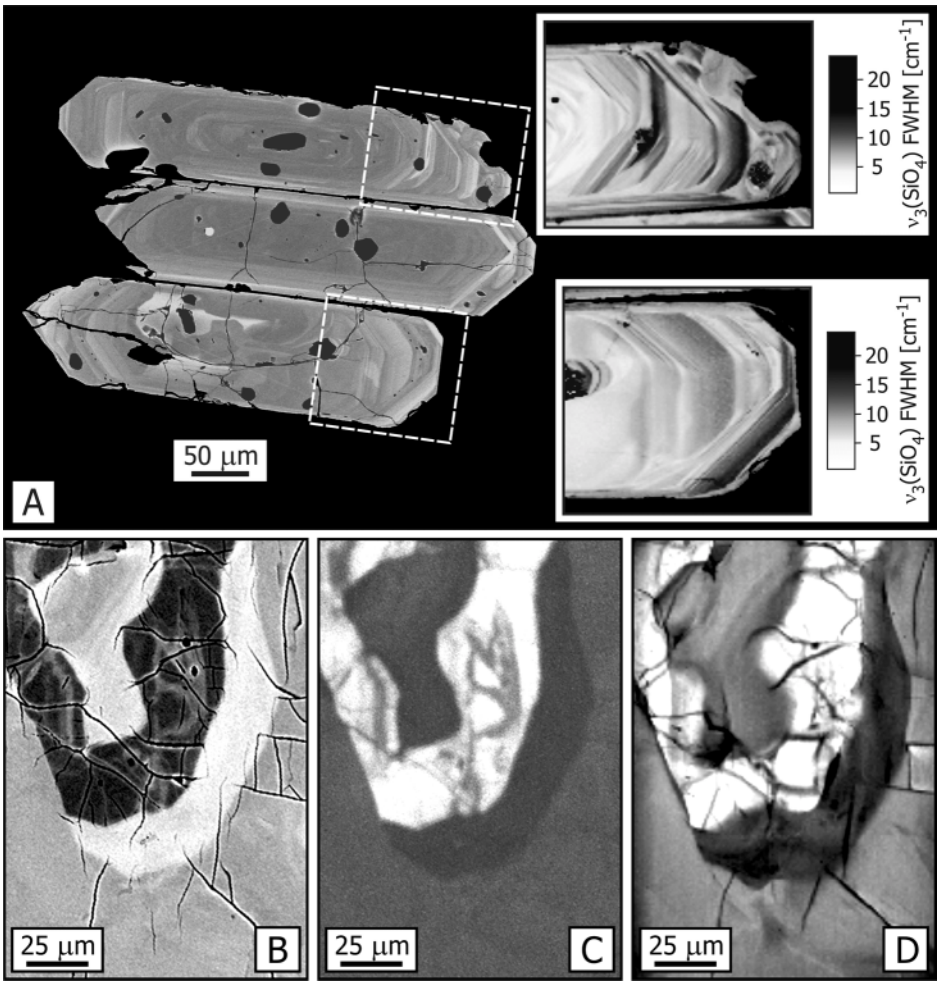

Figure 15. Two examples for the application of Raman microprobe analysis for revealing internal structures of zircon crystals. (A) Backscattered electrons image and two Raman maps obtained from of a group of zircon crystals from the Gold Butte block, Nevada (for sample description see Reiners et al. 2002). (B) Backscattered electrons image a heterogeneous area in a zircon from the Adirondack Mountains, New York State (cf. Figs. 4A and 4B in Nasdala et al. 2002a). (C) Cathodoluminescence image of the same area as in B. (D) Raman map of the same area as in B, generated from ~22,000 spectra (bright = narrow-band widths, well ordered, dark = broad-band widths, disordered). The three Raman-based images (in A and D) show the lateral distribution of the broadening of the $\nu_3(SiO_4)$ Raman band and are thus virtually maps of the crystallinity.

radiation induced color centers (Burns 1993, Anderson and Payne 1998). Colors of crystalline to moderately radiation-damaged zircon samples range from colorless to pale brown, brown, olive, yellow, orange, green and blue. Highly metamict zircon samples are often dark brownish to almost black (in early papers described as "cyrtolith" or "malacon"), but may also have gemstone quality, then typically showing bottle-green color. Early optical absorption studies on natural zircon were pioneered by gemologists for identification purposes. Anderson (1971) and Anderson and Payne (1998) gave overviews of the respective literature.

Cations affecting the color of zircon. It is well known that a large variety of ions can be incorporated into the zircon lattice. Among them, cations with partly filled valence electron shells (transition metals, lanthanides, actinides and REE) give rise to coloration. A number of these

species has been the subject for detailed optical investigations in the past, and these studies are summarized in the following. Accordingly, this subchapter deals with crystal field transitions. For the theoretical principles and a comprehensive overview, the reader is referred to the basic literature (e.g., Ballhausen 1962, Figgis 1966, Lever 1968, Newman 1971, Schläfer and Gliemann 1980, Lever 1984, Newman and Ng 1989). Applications of the crystal-field theory in geosciences are, for instance, given in the reviews by Burns (1970, 1993) and Langer (1988, 1990). Books and articles reviewing mineral spectroscopy along with an extensive list of optical mineral data were compiled by Rossman (1988). Lever (1968, 1984) compiled extensive data about inorganic and organic substances.

Anderson and Payne (1940) attributed the visible absorption spectrum of natural zircon to uranium impurities. The polarization behavior of synthetic U^{4+}-doped zircon at low temperatures was first studied by Richman et al. (1967) who found that tetravalent uranium was substituting for Zr^{4+} (Fig. 16) Absorption bands were observed in the spectral range 23700 to 4850 cm^{-1} and were assigned to their respective transitions. Mackey et al. (1975) proposed an alternative band assignment, and Vance and Mackey (1978) undertook a study to reproduce the absorption spectrum of U^{4+} in the isomorphous lattices of hafnon and thorite. However, no significant information was obtained on the validity of the previous interpretation, which is still under debate. Phenomenologically, the spectrum of synthetic U^{4+}-doped zircon is widely similar to those of natural zircon, though the latter show often broadened bands due to radiation damage (e.g., Anderson 1963). Vance and Anderson (1972a,b) performed detailed studies on natural radiation damaged zircon and found, beside the U^{4+} spectrum, additional absorption bands that were associated with U^{4+} in cubic or tetragonal ZrO_2. This interpretation was supported by the observation that after heat-treatment, ZrO_2 had formed and the additional lines were also intensified. Later, Vance (1974) extended these investigations into the IR spectral range and described further bands of U^{4+}-bearing ZrO_2. Vance and Mackey (1974) found two additional bands in some absorption spectra of natural U-bearing zircon in the infrared region at 9030 and 6700 cm^{-1}, which were attributed to the presence of U^{5+} (cf. Fig. 17). These same authors have also studied synthetic, U-doped zircon (Vance and Mackey 1975, 1978). Previous results for natural zircon were confirmed and it was shown that the U^{5+} is only remotely

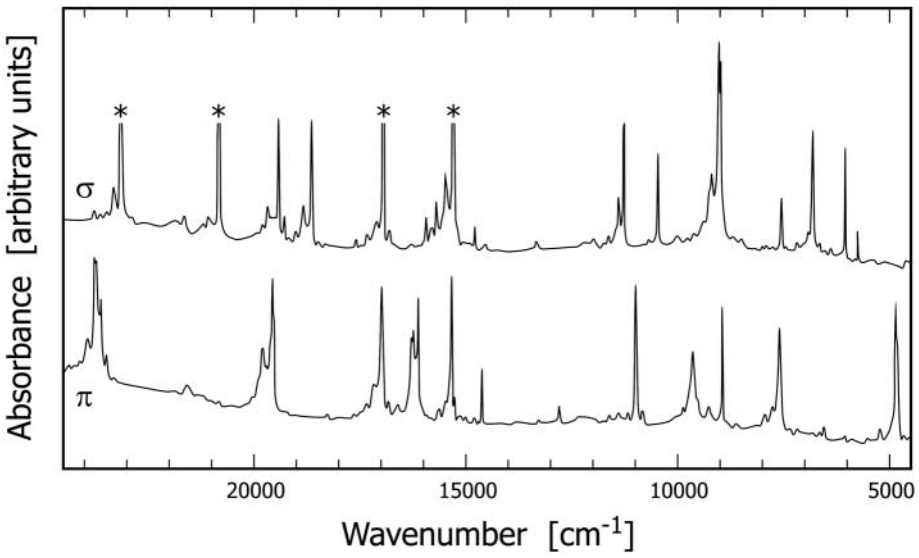

Figure 16. Absorption spectra of U^{4+} in zircon at 4.2 K for the two polarizations σ (***E*** ∥ *c* and ***H*** ⊥ *c*) and π (***E*** ⊥ *c* and ***H*** ∥ *c*), obtained from a synthetic zircon crystal doped with uranium (after Richman et al. 1967, redrawn). Bands marked with an asterisk were too intense. The absorption edge is not shown in the spectra but was reported at ~33000 cm^{-1} in the original paper.

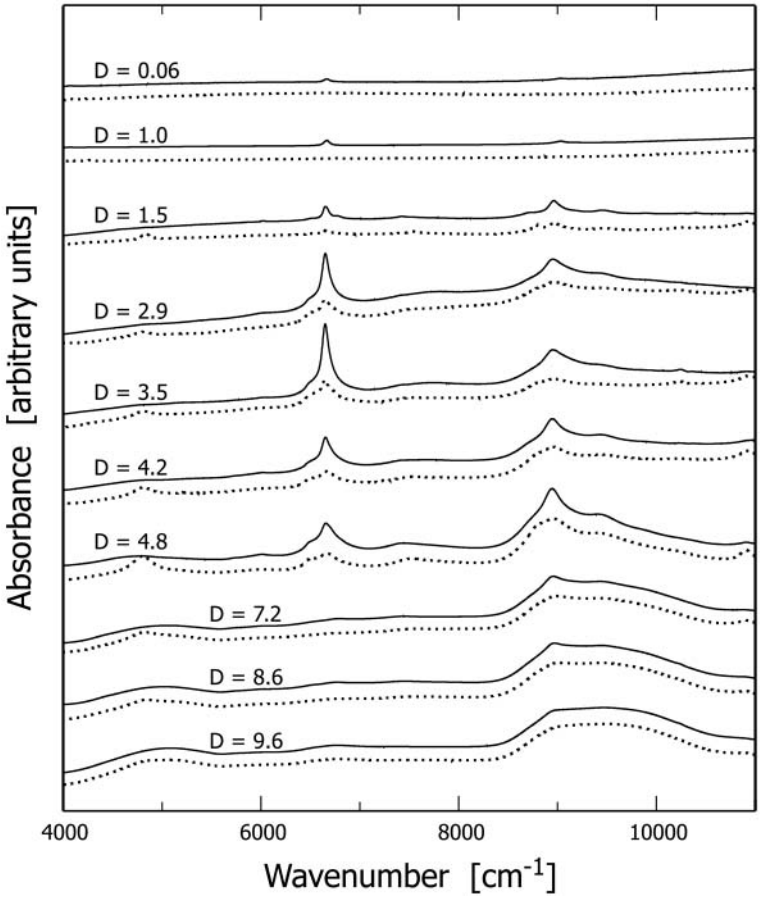

Figure 17. Absorption spectra in the near infrared range obtained from zircon crystals from Sri Lanka having different degrees of radiation damage (redrawn after Zhang et al. 2002). Solid graphs, $\boldsymbol{E} \perp c$, dotted graphs, $\boldsymbol{E} \parallel c$. Spectra are stacked for more clarity of the presentation. Doses are given as in Figure 8. The bands at 6668 and 9030 cm^{-1} are assigned to U^{5+} absorption centers.

charge-compensated by trivalent ions. Zhang et al. (2002) investigated effects of radiation damage and thermal annealing on uranium ions in crystalline and metamict zircon. They found that U^{4+} and U^{5+} signals have different responses to radiation damage. Tetravalent uranium becomes the dominate component in the amorphous phase. Zhang et al. (2002) concluded that due to ionization, the valence of uranium ions may change during the metamictization process.

Fielding (1970) investigated natural zircon that exhibited red colored zones. He reported unpolarized spectra and attributed a broad absorption band around 20000 cm^{-1} to Nb^{4+} substituting for Zr^{4+}. The low energy wing of this band extends into the visible spectral region causing the red color. Other observed spectral features around 15000 to 6000 cm^{-1} were ascribed to uranium, rare earths and iron, but no further details were given. Vance and Mackey (1975) argued that two features of the spectrum at 9000 and 6700 cm^{-1} arise due to U^{5+} (see above).

Belletti et al. (1995) synthesized Cr-doped zircon. The crystals exhibited bluish to greenish color. Polarized absorption spectra, recorded in the spectral region 25000 to 6000 cm^{-1} at various temperatures between 10 K and 300 K, were interpreted on the basis of local D_{2d} symmetry for Cr^{4+} hosting on the Si^{4+} site. The intense absorption bands around 9600-12500 cm^{-1}, 15000-19500 cm^{-1},

and 20500-24000 cm^{-1}, were assigned to spin allowed d-d transitions. However, Gaft et al. (2000c) investigated synthetic Cr-doped zircon using luminescence spectroscopy and found no evidence of Cr^{4+}, rather they found Cr^{3+} and Cr^{5+}. Gaft et al. (2000c) concluded that one possible mechanism of charge compensation is a double substitution Cr^{3+}–Cr^{5+} within two Zr^{4+}–Si^{4+} neighbors of the zircon lattice.

Synthetic zircon doped with vanadium exhibits a blue color, which was attributed to V^{4+} substituting for Zr^{4+} (Booth and Peel 1962). Note that this assignment is contradictory with the Raman results of De Waal et al. (1996) discussed above. Booth and Peel (1962) argued that tri- and pentavalent vanadium may also contribute to the blue coloration. To clarify this, Demiray et al. (1970) measured reflectance spectra of powdered, synthetic V-doped zircon. They reported three broad absorption bands at 37500, 16000 and 6750 cm^{-1}, which they assigned to spin-allowed d-d transitions based on their crystal field analysis for a local D_{2d} symmetry. A shoulder near 13000 cm^{-1} was interpreted as spin-forbidden transition. The absorption edge was observed at around 48000 cm^{-1}. The results of Demiray et al. (1970) seem somewhat questionable. The absorption edge of pure zircon lies around 33000 cm^{-1} (e.g., Richman et al. 1967) and it is well known that it shifts to lower energies due to cation substitutions. For instance, Vance (1974) reported the absorption edge at 23800 cm^{-1}. Silicates without any significant content of transition metal ions generally show an absorption edge around 35000 cm^{-1}. At higher energies the metal-oxygen charge transfer already causes total absorption. Therefore, the reported spin-allowed transition at 37500 cm^{-1} reported by Demiray et al. (1979) is most probably an artifact.

Although Np^{4+} and Pu^{4+} were not found in natural samples, they will be briefly mentioned here. Polarized optical absorption spectra in conjunction with EPR investigations were conducted at low temperature (4.2 K) on Np^{4+} and Pu^{4+} in single zircon crystals by Poirot et al. (1988, 1989). The energy levels were assigned on a basis of local D_{2d} symmetry site for both ions, thus substituting for Zr^{4+} analogous to U^{4+}.

Future needs. The available data on absorption spectroscopic studies are scarce, especially quantitative ones. This might perhaps be due to circumstances that limit the quality of absorption spectra, as for example cases in which the respective cation of interest has only trace concentration, superposition of absorption lines or problems in the identification of electronic transitions. The assignment of the absorption bands to the respective transitions in f-elements is a tedious task. In contrast to most $3d^N$-elements, spin-orbit interaction in f-elements cannot be neglected (e.g., Lever 1968, Marfunin 1979). The U^{4+} ion in zircon is an excellent example for this. Seventy electronic transitions are to be expected for U^{4+} (Richman et al. 1967) but Richman et al. (1967) and Mackey et al. (1975) assigned only 30 U^{4+} bands. Actually, more bands were found in the spectra, but weak bands were supposed to be partly of vibrational origin and were not taken into account. Also, the various parameter sets employed to describe the spectra are the result of different approximations by the respective authors. Accordingly, an improvement of the crystal field model is necessary, and/or comparison with *ab-initio* calculations in the near future will help to clarify the existing uncertainties.

The influence of the radiation damage upon the absorption bands has been recognized (Taran et al. 1990a,b), but has not been investigated in detail. Heat-treatment experiments of radiation damaged zircon addressed to study annealing effects on the behavior of absorption bands are needed. Principally, band narrowing due to "healing" of the structure was already mentioned, but quantitative data are missing. First results in the course of systematic studies on the oxidation state of uranium in metamict and annealed zircon were recently obtained by Zhang et al. (submitted).

The color of natural zircon is in first instance caused by the absorption edge whereas transition metals causing an absorption in the visible spectral region seem to have minor importance in most cases. Especially f-f transitions (actinides and lanthanides) are weak and faint in most natural zircon samples. It is also to be expected that radiation damage in zircon causes the absorption edge to shift into the visible spectral region (for fluorite shown by Trinkler et al. 1993, for biotite shown by Nasdala et al. 2001c). It is clear that more detailed data on the various radiation-induced color centers are needed. Absorption spectroscopy will prove useful for this purpose, especially

when employed in combination with other spectroscopic techniques.

Mössbauer spectroscopy

Only a few attempts have been made thus far to employ ^{57}Fe Mössbauer spectroscopy to the investigation of the valence and structural position of iron ions when incorporated in the zircon lattice. It is well known that natural zircon commonly contains iron as a trace element in the range up to a few hundred ppm. Zircon analyses with significantly higher Fe content have occasionally been reported (e.g., Nechaev et al. 1986, Pointer et al. 1988) but it is generally agreed that exceptionally high iron concentrations are most probably due to finely dispersed inclusions of Fe-phases rather than extensive Fe substitution into the zircon structure.

Berry et al. (1996) observed the simultaneous presence of two iron species in Mössbauer spectra of synthetic $ZrSiO_4$ doped with 0.2-1.8 wt % Fe: a Fe^{3+} doublet interpreted as representing iron substitution in the zircon structure and a Fe^{3+} sextet due to the presence of hematite inclusions. To avoid the Mössbauer signal of incorporated Fe-bearing minerals, Blaum and Nasdala (1999) studied nine natural zircon samples with low Fe concentrations <200 ppm. They found that ^{57}Fe Mössbauer spectra of well crystallized and metamict zircon showed wide similarity, with ferric iron always being the dominant Fe species. Hawthorne et al. (1991) concluded from the Mössbauer spectra of one crystalline and one metamict titanite that the accumulation of radiation damage might be accompanied by partial $Fe^{3+} \rightarrow Fe^{2+}$ reduction. In contrast, Blaum and Nasdala (1999) found no correlation between the degree of radiation damage and the Fe^{2+}/Fe^{3+} ratio in zircon.

The assignment of the various iron species to certain lattice sites is still under debate. Mössbauer spectra of natural low-Fe zircon samples are dominated by a Fe^{3+} doublet with relatively low quadrupole splitting of Δ = 0.30-0.32 mm/s [Fe^{3+}(I) in Fig. 18], which corresponds to a highly symmetric site. Its chemical shift of δ = 0.2 mm/s (relative to α-Fe) suggests tetrahedrally coordinated Fe. The best candidate for this $^{[4]}Fe^{3+}$ seems the nearly symmetric, empty [4]-coordinated site in the zircon lattice (cf. Finch et al. 2001) with a cation–oxygen distance of 1.84 Å (Fig. 18). Incorporation of Fe^{3+} at the comparably "narrow" Si sites (Si–O bond distance 1.62 Å) seems more difficult and, if possible at all, it must be accompanied by significant widening and distortion of tetrahedra. Blaum and Nasdala (1999) have also speculated that both ferrous and ferric iron could occupy the empty [6]-coordinated site in the zircon lattice (Robinson et al. 1971; Fig. 19). Hypothetical Fe substitution at the $^{[8]}$Zr site is only possible for the (larger) Fe^{2+}. It seems, however, unlikely that the occasionally found, low Fe^{2+} portion in natural zircon is [8]-coordinated. Such $^{[8]}Fe^{2+}$ species is expected to show large quadrupole splittings (Δ ~ 3.5 mm/s, Burns 1994), which was, however, not observed by Blaum and Nasdala (1999; cf. Fig. 18).

All of the above assignments, however, are somewhat questioned by widely similar parameters for the main Fe^{3+} doublet in Mössbauer spectra obtained from little and highly metamict zircon. This observation would imply that the short-range order around the Fe sites remains unaffected by the radiation damage whereas the short-range order of other sites decreases. It must therefore be cautiously considered that even in low-Fe zircon, iron might be present as a sub-micrometer phase or cluster, rather than being incorporated in the zircon structure.

Electron paramagnetic resonance

General remarks. Electron paramagnetic resonance (also electron spin resonance, ESR) is a spectroscopic method that detects chemical species with unpaired electrons. The technique is based on the interaction between the magnetic moment of these unpaired electrons and microwaves in an external magnetic field. Resonant microwave absorption occurs between the energy levels of the ground state of the unpaired electrons which are split in the EPR spectrometer's uniform magnetic field (usually 0-1 T). Electron paramagnetic resonance spectroscopy is a very powerful method for investigating the detailed physical properties, structural position and local

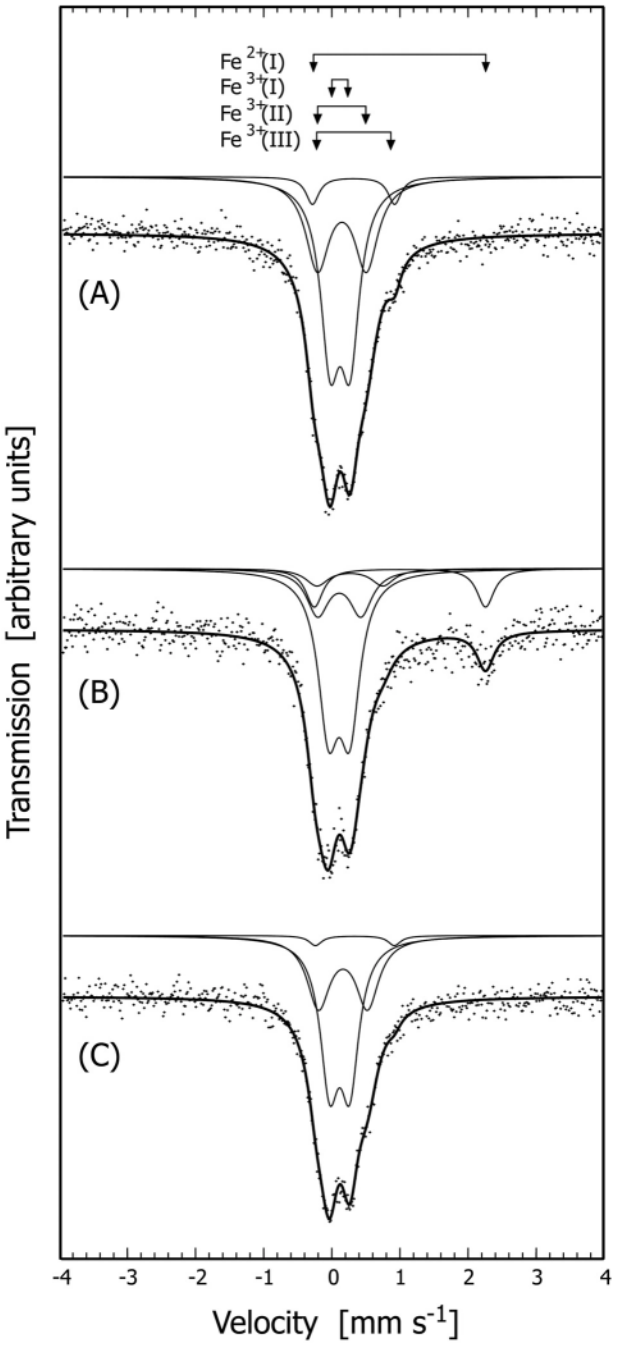

Figure 18. Comparison of three ^{57}Fe Mössbauer spectra (stacked) of natural zircon samples (Blaum and Nasdala 1999, P Blaum, unpublished). (A) Crystalline zircon from Miask, Ural Mountains, without detectable ferrous iron. (B) Crystalline zircon from Miask, Ural Mountains, showing doublets of ferric and ferrous iron. (C) Highly metamict zircon from Sri Lanka (UO_2 ~ 0.86 wt %). Note the wide similarity (quadrupole splitting, chemical shift, relative intensity) of fitted Fe^{3+} and Fe^{2+} doublets (assignment on the top), which are apparently unaffected by the different degrees of radiation damage.

environment of paramagnetic defects in ionic materials. There are two types of paramagnetic centers in such materials, namely, impurities of paramagnetic ions and radiation-induced electron- and hole-centers. Paramagnetic ions are transition ions in the relevant valence state with unpaired *d*- and *f*-electrons. In some cases, these ions reach the paramagnetic valence state after electron or hole capture due to irradiation processes. Especially radiation-induced intrinsic electron-hole centers can be investigated effectively by means of EPR as an excellent method for the identification of point defects, their local environment, and kinetics of the processes involving these defects. For the fundamentals of EPR, the reader is referred to the numerous works published on this subject, e.g., Abragam and Bleaney (1969), Wertz and Bolton (1972), Marfunin (1979) and Calas (1988).

Impurities of paramagnetic ions. In the unit cell there are four ZrO_8 and four SiO_4^{4-} groups each set of which are both crystallographically (D_{2d}) and magnetically equivalent. Due to the fact that the neighboring [SiO_4] tetrahedra are equally divided into two non-equivalent sets with different Zr-O bond lengths (2.13 Å and 2.27 Å, respectively) there are two types of O-sites. From EPR data, most of the non-formula paramagnetic ions were assigned to the "dodecahedral" Zr site. Various rare-earth ions (4*f*-ions), which play a crucial role in the CL and TL spectra of zircon, were found substituting for Zr^{4+} and forming paramagnetic centers.

One of the first described paramagnetic centers in zircon is Gd^{3+} (Hutton and Troup 1964,

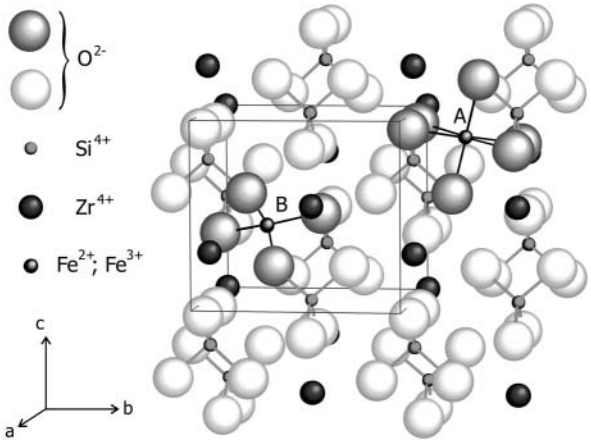

Figure 19. The crystal structure of zircon. Hypothetical iron incorporation at normally empty sites in the structure is shown. (A) Six-coordinated site, slightly elongated parallel to the *c*-axis (see Robinson et al. 1971). (B) Highly symmetric, four-coordinated site (see Finch et al. 2001). These two sites could also be acceptors for the incorporation of other medium-sized cations.

Abraham et al. 1969; Fig. 20). Further REE centers, not observable with EPR at room temperature, are Er^{3+} (Valishev et al. 1965), Dy^{3+} (Ball 1971), Tm^{2+} (Bershov 1971) and Tb^{4+} (Hutton and Milne 1969). Diamagnetic incorporated *d*- and *f*-ions can be transformed to the paramagnetic state by trapping of an electron due to self-irradiation as well as external irradiation. These charge transfer processes modify the defect structure forming electron- or hole-centers with anomalous valence state of the incorporated ion. E.g., the Tb^{4+} forms by electron-hole capture on Tb^{3+}. The electron-hole is not only occupying the terbium position but also the nearest oxygen site. The presence of two different oxygen sites in the zircon lattice causes the appearance of two physically different EPR spectra (Bershov 1971). The paramagnetic Nb^{4+} center was found in natural (Vinokurov et al. 1963) and synthetic Nb-doped zircon (Di Gregorio et al. 1980). It results from electron capture by Nb^{5+} occupying a Zr^{4+} site. The same type is the Ti^{3+} center (Samoilovich et al. 1968, Solntsev and Shcherbakova 1972, Claridge et al. 1995). For both centers hyperfine interaction with a Y^{3+} or a P-ion which isomorphously replaces a next-nearest-neighboring Zr^{4+} ion were reported for synthetic crystals irradiated at 77 K (Solntsev and Shcherbakova 1974, Claridge et al. 1997, Tennant and Claridge 1999). A Mo^{5+} center on Zr^{4+} site was described for synthetic zircon crystals (Krasnobayev et al. 1988). Further paramagnetic d-ions incorporated at the Zr^{4+} site in zircon are Fe^{3+} (Vinokurov et al. 1972), V^{4+} (Ball and Wanklyn 1976) and in synthetic doped crystals Np^{4+} (Poirot et al. 1988). Interestingly so far neither in natural nor in synthetic zircon paramagnetic uranium centers were described with the EPR.

Besides the paramagnetic ions which were in natural crystals mostly assigned to the "dodecahedral" Zr^{4+} site especially in 3*d*- and 4*d*-ion doped synthetic crystals the "tetrahedral" Si^{4+} site or a possible incorporation on both sites was suggested for Ti^{3+} (Claridge et al. 1999a), Mo^{5+} (Krasnobayev et al. 1988, Eftaxias et al. 1989), V^{4+} (Di Gregorio et al. 1982), Cr^{3+} (Claridge et al. 1999b) and Fe^{3+} (Ball and van Wyk 2000). Berry et al. (1996) reported that iron in doped zircon is accommodated as α-Fe_2O_3 inclusions and as Fe^{3+} centers in low symmetric rhombic sites, at higher iron concentration also in axial sites. Such normally empty, axial sites in the zircon structure having [6]- and [4]-coordination were described by Robinson et al. (1971) and Finch et al. (2001), respectively (Fig. 19 and Mössbauer spectroscopy above). Both spectra of Fe^{3+} on the Zr^{4+} site and on the Si^{4+} site were found by Vinokurov et al. (1972) only in natural zircon crystals from kimberlites. The incorporation of paramagnetic *d*-ions at these structural sites must be accompanied by signifi-

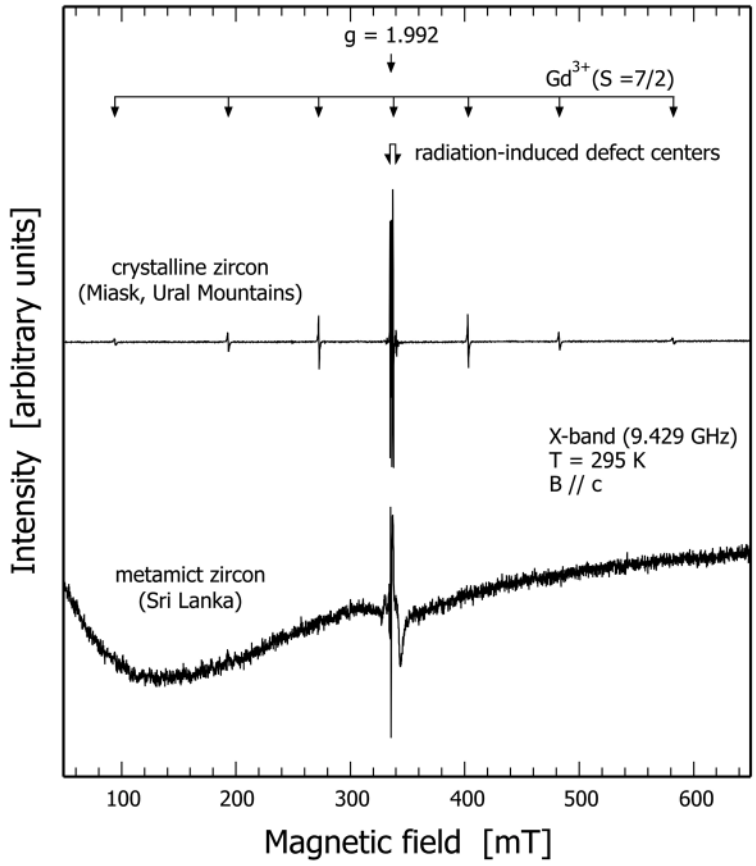

Figure 20. Typical EPR spectra of little and highly radiation-damaged, natural zircon (M Plötze and L Nasdala, unpublished). Both of the spectra are dominated by signals of radiation-induced electron-hole centers. In addition, the upper spectrum (crystalline zircon) shows the signal of Gd^{3+}. The latter is not resolved in the EPR spectrum of metamict zircon, which is probably due to broadening of the crystal-field parameters and accompanying broadening of the spin-Hamiltonian terms.

cant distortions of both the octahedron and tetrahedron but appears probable especially under extreme crystallization conditions e.g. in kimberlites or high doping synthesis. However, their unequivocal assignment to certain structural sites is presently impossible from EPR data and need further experiments, e.g. measurements of the interactions with O-ligands in ^{17}O enriched samples or EXAFS measurements.

Intrinsic radiation-induced paramagnetic centers. Besides the paramagnetic centers related to paramagnetic ions, a large number of intrinsic paramagnetic species in zircon was observed and characterized by EPR. These centers are formed by trapping of electrons or electron-holes in the zircon lattice as a result of natural self-irradiation or artificial ionizing radiation. The number and nature of the paramagnetic defects depend on the impurity content, the previous heat treatment of the crystal, the type of the radiation, the temperatures during irradiation and potential subsequent heating and, finally, the temperature at which the EPR measurements are performed. Most of the known radiation-induced paramagnetic electron-hole centers are thermally unstable and anneal at room temperature.

Irradiation causes the formation of the d^1 Zr^{3+} electron center on the Zr^{4+} site, which is therefore a prominent center in irradiated crystals. Recent studies showed that the Zr^{3+} center results from trapping of an electron at a Zr^{4+} site stabilized by a P^{5+} ion at a closely neighbored Si^{4+} site

(Claridge et al. 2000b).

As the only anion in the ideal zircon crystal lattice, O^{2-} serves as the only host for electron holes to be formed during ionizing irradiation. There are two non-equivalent oxygen sites and, correspondingly two possible types of O-sites for trapping of paramagnetic electron-holes in the zircon lattice. Oxygenic hole-centers result from trapping of an electron-hole in a ligand oxygen *p* orbital, which is stabilized by a closely neighbored impurity cation. For example, the negative charge created by a trivalent ion substituted at a neighboring Si^{4+} or Zr^{4+} site assists trapping of the oxygenic hole after ionizing irradiation (Claridge et al. 2000a, and references therein). The $[AlO_4]^0$ center is a hole-center, with the hole on a short bond ligand O position, interacting with a $^{27}Al^{3+}$ nucleus located in an adjacent Si^{4+} lattice position (Solntsev and Shcherbakova 1973, Claridge et al. 1994b). The precursor state for this center is the diamagnetic $[AlO_4]^-$ associated with an adjacent charge compensating cation M^+ (H^+, Li^+, Na^+). In contrast to alpha-quartz, where the same center was observed (Nuttall and Weil 1981a,b), in zircon a M^+ compensator was not detected inferring either the compensation is remote or the compensator is able to diffuse away even by irradiation at 77 K. A further center of this type is $[BO_4]^0$ (Walsby et al. 2000). The center $[SiO_4]^{3-}$-Y^{3+}, found in natural zircon numbers also among this group, however, here a stabilizing yttrium is incorporated at the zirconium site (Bershov 1971, Vinokurov et al. 1971, Barker and Hutton 1973, Danby and Hutton 1980, Claridge et al. 2000a).

The group of radiation-induced electron- or hole-centers which are related to zirconium and oxygen vacancies are described by the formula $[SiO_m]^{n-}$ (e.g., Samoylovich et al. 1968, Solntsev et al. 1974, Krasnobayev et al. 1988, Kalinichenko et al. 1990, Claridge et al. 2000a, Laruhin et al. 2002). The hole-centers were produced by trapping of an electron-hole on the ligand oxygen *p* orbital. Two distinct hole-centers $[SiO_2]^{3-}$ according to the two types of O-sites for trapping of paramagnetic holes were described by Claridge et al. (1994). The center with the hole located in a 2p orbital of an oxygen of the $[SiO_4]$-group directed towards the neighboring Zr^{4+} vacancy is reasonably stable even at room temperature (Claridge et al. 1999). The electron-centers $[SiO_4]^{5-}$, $[SiO_3]^{3-}$ and $[SiO_2]^-$ were produced by trapping of an electron at the silicon oxide group. The most important electron-center is represented by $[SiO_4]^{5-}$ (Solntsev et al. 1974). It is moderately stable at room temperature (Laruhin et al. 2002).

As was already mentioned in the previous paragraphs, the radiation-induced paramagnetic centers affect the broadband luminescence emission. They are also influencing the optical absorption behavior. With various techniques of EPR and fission track imaging Kasuya et al. (1990) found a positive correlation between the density of O^- hole-centers, the fission-track density and the red coloring of zircon. A relationship between radiation-induced paramagnetic centers and the red color was described also by Taran et al. (1990b) in combined optical absorption and EPR investigations of zircon from kimberlites.

Other spectroscopic methods

Solid state NMR spectroscopy has been employed to characterize and determine the chemical and physical properties of zircon. Its applications have focused on several research areas. Firstly, ^{29}Si NMR and ^{29}Si magic angle sample spinning (MAS-NMR) techniques were commonly used to investigate and characterize the crystallization or formation of $ZrSiO_4$ from ZrO_2-SiO_2 gel and aqueous sols (Hartman et al. 1990, Tartaj et al. 1994, Bhattacharya et al. 1996, Valéro et al. 1999, Veytizou et al 2000). Secondly, ^{29}Si NMR was employed to study the metamictization process of zircon (Rudnitskaya and Lipova 1972, Kalinichenko et al. 1990, Farana and Salje 2001). Data from ^{29}Si NMR (Kalinichenko et al. 1990, Farana and Salje 2001) showed that α-decay damage causes new signals indicative of partial polymerization. In addition, Kalinichenko et al. (1990) and Valéro et al. (1999) characterized hydrous components in zircon using ^1H NMR. Applications of ^{91}Zr and ^{17}O NMR in zircon are scarce (Bastow 1990, Carlisle et al. 1991), which is probably due to experimental difficulties. Dajda et al. (2003) recently studied the local structure and site occupancies of pure

and vanadium-doped zircon as well as sol-gels with solid-state NMR or MAS NMR spectra of ^{29}Si, ^{17}O, ^{91}Zr and ^{51}V. Their results suggested that vanadium substitution occurs on both the tetrahedral and dodecahedral sites within the zircon lattice with a small preference for the tetrahedral site. These authors also observed a third peak at relatively high vanadium concentration (0.92 mol % V^{4+}) and this was interpreted as a third substitution within the zircon lattice.

There are also a number of papers in which X-ray absorption spectroscopy (i.e. extended X-ray absorption fine structure, EXAFS, X-ray absorption near edge structure, XANES) was employed to study the real structure of radiation-damaged zircon. These studies, as well as the NMR work related to radiation damage phenomena in zircon, are discussed by Ewing et al. (this volume).

ACKNOWLEDGMENTS

We are indebted to Peter Blaum, Jens Götze, John M. Hanchar, Wolfgang Hofmeister, Paul W.O. Hoskin, Andreas Kronz, Peter W. Reiners and Michael Wiedenbeck for providing samples, data, spectra and images. Special thanks are due to Dieter Wolf for many stimulating discussions. Constructive reviews of the manuscript by Michail N. Taran, Glenn Waychunas and Brigitte Wopenka are gratefully acknowledged. Thanks are also due to Wolfgang Zirbs, John M. Hanchar and Christopher M. Fedo for editorial help.

REFERENCES

Abragam A, Bleaney B (1970) Electron Paramagnetic Resonance of Transition Ions. Clarendon Press, Oxford

Abraham MM, Clark GW, Finch CB, Reynolds RW, Zeldes H (1969) Ground-state splitting of trivalent Gd and Cm in $ZrSiO_4$, $HfSiO_4$, and $ThSiO_4$, determined by ESR. J Chem Phys 50:2057-2062

Aines RD, Rossman GR (1985) The high temperature behavior of trace hydrous components in silicate minerals. Am Mineral 70:1169-1179

Aines RD, Rossman GR (1986) Relationship between radiation damage and trace water in zircon, quartz, and topaz. Am Mineral 71:1186-1193

Akhmanova MV, Leonova LL (1961) Investigation of the metamict decay of zircon with the aid of infrared absorption spectra. Geokhimiya 1961:401-414 (in Russian)

Akhmanova MV, Leonova LL (1963) Investigation of the metamict decay of silicates with the aid of infrared spectroscopy. Trudy Mineral Muzeya AN SSSR im A.E. Fersmana 14:3-31 (in Russian)

Alexanian C, Morel P, Le Bouffant L (1966) Infrared absorption spectra of natural minerals. Bull Soc Fr Ceram 71:3-38

Anderson BW (1963) Absorption spectra and properties of metamict zircons. J Gemmol 9:1-6

Anderson BW (1971) Gem Testing. Butterworths, London

Anderson BW, Payne CJ (1940) Recent investigations of zircon. IV. The absorption spectrum. Gemmologist 9:1-5

Anderson BW, Payne J (1998) Absorption spectra of zircon. *In* The Spectroscope and Gemmology. Mitchell RJ (ed) Gemstone Press, Woodstock, Vermont

Balan E, Neuville DR, Trocellier P, Fritsch E, Muller J-P, Calas G (2001) Metamictization and chemical durability of detrital zircon. Am Mineral 86:1025-1033

Ball D (1971) Paramagnetic resonance of Er^{3+} and Dy^{3+} in natural single crystals of zircon. Phys status solidi (b) 46:635-641

Ball D, van Wyk JA (2000) The electron paramagnetic resonance of Fe^{3+} observed in two axial sites in synthetic single crystals of zircon ($ZrSiO_4$). Phys status solidi (b) 218:545-551

Ball D, Wanklyn BM (1976) Coloured synthetic zircon crystals. Phys status solidi (a) 36:307-316

Ballhausen CJ (1962) Introduction to Crystal Field Theory. McGraw Hill, New York

Bastow TJ (1990) ^{91}Zr nuclear qundrupole coupling in zircon ($ZrSiO_4$). J Phys: Condens Matter 2:6327-6330

Belletti A, Borromei R, Oleari L (1995) Absorption spectra of zircon crystals doped with Cr(IV): $ZrSiO_4$:Cr^{4+}. Inorg Chim Acta 235:349-355

Barker PR, Hutton DR (1973) A colour centre in natural zircon. Phys status solidi (b) 60:k109-k111

Benisek A, Finger F (1993) Factors controlling the development of prism faces in granite zircons: a microprobe study. Contrib Mineral Petrol 114:441-451

Berry FJ, Eadon D, Holloway J, Smart LE (1996) Iron-doped zirconium silicate. Part 1: The location of iron. J Mater Chem 6:221-225

Bershov LV (1971) Isomorphism of Tb^{4+}, Tu^{2+} and Y^{3+} in zircon. Geokhimiya 1971:48-53 (in Russian)

Bhattacharya AK, Hartridge A and Mallick KK 1996 An X-ray diffraction and NMR study into the mechanism of zircon formation from aqueous sols. J Mater Sci 31:5873-5876

Biagini R, Memmi I, Olmi F (1997) Radiation damage in zircons. N Jb Mineral Mh 1997:257-270
Bibikova EV, Senin VG, Legkova GA (1991) Geochemical and age heterogeneity of accessory zircon from the Novopavlovskij Complex (Ukrainain shield). Geokhimiya 1991:1426-1436
Blanc P, Baumer A, Cesbron F, Ohnenstetter D, Panczer G, Remond G (2000) Systematic cathodoluminescence spectral analysis of synthetic doped minerals: anhydrite, apatite, calcite, fluorite, scheelite and zircon. *In* Cathodoluminescence in Geosciences. Pagel M, Barbin V, Blanc P, Ohnenstetter D (eds) Springer, Berlin–Heidelberg, p 126-160
Blaum P, Nasdala L (1999): The incorporation of iron in zircon, $ZrSiO_4$: a ^{57}Fe Mössbauer study. Eur J Mineral 11:35
Booth CA, Peel GN (1962) Preparation and properties of some zircon stains. Trans Brit Ceram Soc 61:359-400
Burns RG (1970) Mineralogical Applications of Crystal Field Theory: 1st Edn. Cambridge University Press, Cambridge
Burns RG (1993) Mineralogical Applications of Crystal Field Theory: 2nd Edn. Cambridge University Press, Cambridge
Burns RG (1994) Mineral Mössbauer spectroscopy: correlations between chemical shift and quadrupole splitting parameters. Hyperfine Interactions 91:739-745
Calas G (1988) Electron paramagnetic resonance. Rev Mineral 18:513-571
Carlisle BB, Brown RJC, Bastow TJ (1991) Zirconium-91 NQR in zircon. J Phys: Condens Matter 3:3675-3676
Caruba R, Baumer A, Turco G (1975) Nouvelles syntheses hydrothermales du zircon: substitutions isomorphiques, relation morphologie-milieu de croissance. Geochim Cosmochim Acta 39:11-26
Caruba R, Baumer A, Ganteaume M, Iacconi P (1985) An experimental study of hydroxyl groups and water in synthetic and natural zircons: A model of the metamict state. Am Mineral 70:1224-1231
Cesbron F, Ohnenstetter D, Blanc Ph, Rouer O, Sichere MC (1993) Incorporation de terres rares dans des zircons de synthese: etude par cathodoluminescence. C R Acad Sci Paris 316(II):1231-1238
Chatagnon B, Galland D, Gloux P, Meary A (1982) L'ion paramagnetique Tm^{2+} dans la fluorit. Mineral Deposita 17:411-422
Claridge RFC, Mackle KM, Sutton GLA, Tennant WC (1994a) Zircon EPR revisited: 10 K EPR of three low-symmetry centres in irradiated zircon (zircon silicate). J Phys: Condens Matter 6:3429-3436
Claridge RFC, Mackle KM, Sutton GLA, Tennant WC (1994b) 10 K EPR of an oxygen-hole aluminium centre, $[AlO_4]^0$, in x-irradiated zircon, $ZrSiO_4$. J Phys: Condens Matter 6:10415-10422
Claridge RFC, McGavin DG, Tennant WC (1995) 10 K electron paramagnetic resonance of a d^1 Ti^{3+} centre in X-irradiated zircon (zirconium silicate). J Phys: Condens Matter 7:9049-9060
Claridge RFC, Taylor KC, Tennant WC, Walsby CJ (1997) X-band electron paramagnetic resonance of a new Ti^{3+} centre in x-irradiated zircon. J Phys: Condens Matter 9:3075-3080
Claridge RFC, Lees NS, Tennant WC, Walsby CJ (1999a) Two Ti^{3+} centres studied by X-band electron paramagnetic resonance at 10 K in zircon. J Phys: Condens Matter 11:3571-3580
Claridge RFC, Tennant WC, Schweizer S, Spaeth J-M (1999b) Structural models for room temperature stable radiation-induced centers in zircon. J Phys: Condens Matter 11:8579-8589
Claridge RFC, Lees NS, Tennant WC, Walsby CJ (2000a) Oxygenic-hole centres in X-irradiated zircon: 10 K EPR studies. J Phys: Condens Matter 12:1431-1440
Claridge RFC, Tennant WC, Walsby CJ, Schweizer S, Spaeth J-M (2000b) An EPR/ENDOR investigation of a $[ZrPO_4]$ centre in x-irradiated zircon: the Zr(α) centre. J Phys: Condens Matter 12:1421-1430
Coleman RC, Erd RC (1961) Hydrozircon from the Wind River formation, Wyoming. U S Geol Surv Bull 424C:297-300
Colombo M, Chrosch J, Biagini R, Memmi I (1999) An IR analysis of the role of SiO_4 tetrahedra in thermally annealed $ZrSiO_4$. N Jb Mineral Mh 1999:113-122
Connelly JN (2000) Degree of preservation of igneous zonation in zircon as a signpost for concordancy in U/Pb geochronology. Chem Geol 172:25-39
Dajda N, Dixon JM, Smith ME (2003) Atomic site preferences and structural evolution in vanadium-doped $ZrSiO_4$ from multinuclear solid-state NMR. Phys Rev B (in press)
Danby RJ, Hutton DR (1980) A new radiation defect center in natural zircon. Phys status solidi (b) 98:k125-k128
Dawson P, Hargreave MM, Wilkinson GF (1971) The vibrational spectrum of zircon ($ZrSiO_4$). J Phys C: Solid State Phys 4:240-256
Deliens M, Delhal J, Tarte P (1977) Metamictization and U-Pb systematics—A study by infrared absorption spectrometry of Precambrian zircons. Earth Planet Sci Lett 33:331-344
Demiray T, Nath DK, Hummel F (1970) Zircon-vanadium blue pigment. J Am Ceram Soc 53:1-4
De Waal D, Heynd AM, Pretorius G, Clark RJH (1996) Raman spectroscopic investigations of ZrSiO4:V4+, the blue vanadium pigment. J Raman Spectros 27:657-662
Di Gregorio S, Greenblatt M, Pifer JH (1980) ESR of Nb^{4+} in zircon. Phys status solidi (b) 101:k147-k150
Di Gregorio S, Greenblatt M, Pifer JH, Sturge MD (1982) An ESR and optical study of V^{4+} in zircon-type crystals. J Chem Phys 76:2931-2937
Eftaxias K, Fielding PE, Lehmann G (1989) Mo^{5+} in synthetic zircon crystals. Chem Phys Lett 160:36-38
Farmer VC, editor (1975) The Infrared Spectra of Minerals. Mineralogical Society, London
Farnan I, Salje EKH (2001) The degree and nature of radiation damage in zircon observed by ^{29}Si nuclear magnetic

resonance. J Appl Phys 89:2084-2090
Fielding PE (1970) The distribution of uranium, rare earths, and color centers in a crystal of natural zircon. Am Mineral 55:428-440
Figgis BN (1966) Introduction to Ligand Fields. Interscience, New York
Finch RJ, Hanchar JM, Hoskin PWO, Burns PC (2001) Rare earth elements in synthetic zircon: Part 2. A single-crystal X-ray study of xenotime substitution. Am Mineral 86:681-689
Frondel C (1953) Hydroxyl substitution in thorite and zircon. Am Mineral 38:1007-1018
Frondel C, Collette R (1957) Hydrothermal synthesis of zircon. Am Mineral 42:759-765
Gaft M (1992) Application of thermal treatment of zircon for the interpretation of luminescence centres. J Thermal Anal 38:2281-2290
Gaft M, Panczer G, Reisfeld R, Shinno I (2000a) Laser-induced luminescence of rare-earth elements in natural zircon. J Alloys Com 300-301:267-274
Gaft M, Panczer G, Reisfeld R, Shinno I, Champagnon B, Boulon G (2000b) Laser-induced Eu^{3+} luminescence in zircon ZrSiO4. J Luminesc 87-89:1032-1035
Gaft M, Boulon G, Panczer G, Guyot Y, Reisfeld R, Votyakov, Bulka G (2000c) Unexpected luminescence of Cr^{5+} and Cr^{3+} ions in $ZrSiO_4$ zircon crystals. J Luminesc 87-89:1118-1121
Gaft M, Panczer G, Reisfeld R, Uspensky E (2001) Laser-induced time-resolved luminescence as a tool for rare-earth element identification in minerals. Phys Chem Minerals 28:347-363
Gaft M, Shinno I, Panczer G, Reisfeld R (2002) Laser-induced time-resolved spectroscopy of visible broad luminescence bands in zircon. Mineral Petrol (in press)
Gebauer D (1990) Isotopic systems - geochronology of eclogites. *In* Eclogite Facies Rocks. Carswell DA (ed) Blackie, Glasgow–London, p 141-159
Geisler T, Ulonska M, Schleicher H, Pidgeon RT, van Bronswijk W (2001a) Leaching and differential recrystallization of metamict zircon under experimental hydrothermal conditions. Contrib Mineral Petrol 141:53-65
Geisler T, Pidgeon RT, von Bronswijk W, Pleysier R (2001b) Kinetics of thermal recovery and recrystallization of partially metamict zircon: a Raman spectroscopic study. Eur J Mineral 13:1163-1176
Geisler T, Zhang M, Farna I, Salje EKH (2002) Recrystallzation of heavily metamict zircon under different hydrothermal P-T-t-X conditions. Eur J Mineral 14:51
Gervais F, Piriou B, Cabannes F (1973) Anharmonicity in silicate crystals: Temperature dependence of A_u type vibrational modes in $ZrSiO_4$ and $LiAlSi_2O_6$. J Phys Chem Solids 34:1785-1796
Goldstein JI, Newbury P, Echlin P, Joy DC, Fiori C, Lifshin E (1981) Scanning Electron Microscopy and X-ray Microanalysis. Plenum Press, New York
Gorobets B, Rogozin A (2001) Luminescence Spectra of Minerals (reference book). VIMS, Moscow (in Russian)
Götze J (1998) Principle and advantages of cathodoluminescence microscopy. Microsc Analysis, Eur Ed 55:17-19
Götze J, Kempe U, Habermann D, Nasdala L, Neuser RD, Richter DK (1999) High-resolution cathodo-luminescence combined with SHRIMP ion probe measurements of detrital zircons. Mineral Mag 63:179-187
Gracheva TV, Bibikova EV, Akhmanova MV (1981) Ascertaining of geochronologic role of metamictization degree of zircon using IR spectroscopy. Geokhimiya 1981:274-291 (in Russian)
Granqvist CG, Hunderi O (1978) Optical properties of Ag-SiO_2 cermet films: A comparison of effective-medium theories. Phys Rev B 18:2897-2906
Griffith WP (1970) Raman studies on rock-forming minerals. Part I. Orthosilicates and cyclosilicates. J Chem Soc (A) 1969:1372-1377
Halden NM, Hawthorne FC (1993) The fractal geometry of oscillatory zoning in crystals: Application to zircon. Am Mineral 78:1113-1116
Hanchar JM, Miller CF (1993) Zircon zonation patterns as revealed by cathodoluminescence and backscattered electron images: Implications for interpretation of complex crustal histories. Chem Geol 110:1-13
Hanchar JM, Rudnick RL (1995) Revealing hidden structures: The application of cathodoluminescence and back-scattered electron imaging to dating zircons from lower crustal xenoliths. Lithos 36:289-303
Hanchar JM, Hoskin PWO, Jackson SG, Hinton RW, Thibault Y, Finch RJ, Wolf S, Watson EB, Hemming S, Hanson B, Lindstrom DJ (1997) Rare earth elements and the Ce anomaly in terrestrial zircons. EOS Trans, Am Geophys Union 78:F783
Hanchar JM, Finch RJ, Hoskin PWO, Watson EB, Cherniak DJ, Mariano AN (2001) Rare earth elements in synthetic zircon: Part 1. Synthesis, and rare earth element and phosphorus doping. Am Mineral 86:667-680
Hartman JS, Millard RL and Vance ER 1990 A Si^{29} magic angle spinning NMR and DTA study of thermal crystallization of sphene and zircon gels. J Mater Sci 25:2785-2790
Hawthorne FC, Groat LA, Raudsepp M, Ball NA, Kimata M, Spike FD, Gaba R, Halden NM, Lumpkin GR, Ewing RC, Greegor RB, Lytle FW, Ercit TC, Rossman GR, Wicks FJ, Ramik RA, Sherriff BL, Fleet ME, McCammon C (1991) Alpha-decay damage in titanite. Am Mineral 76:370-396
Hermann J, Rubatto D, Korsakov A, Shatsky VS (2001) Multiple zircon growth during fast exhumation of diamondiferous, deeply subducted continental crust (Kokchetav Massif, Kazakhstan). Contrib Mineral Petrol 141:66-82

Heyns AM, Range KJ, Wildenauer M (1990) The vibrational spectra of $NbBO_4$, $TaBO_4$, $NaNb_3O_8$, and $NaTa_3O_8$. Spectrochim Acta 46A:1621-1628
Hoffman JF, Long JVP (1984) Unusual sector zoning in Lewisian zircons. Mineral Mag 48:513-517
Högdahl K, Gromet L-P, Broman C (2001) Low P-T Caledonian resetting of U-rich Paleoproterozoic zircons, central Sweden. Am Mineral 86:534-546
Hoskin PWO (2000) Patterns of chaos: fractal statistics and the oscillatory chemistry of zircon. Geochim Cosmochim Acta 64:1905-1923
Hoskin PWO, Rodgers KA (1996) Raman spectral shift in the isomorphous series $(Zr_{1-x}Hf_x)SiO_4$. Eur J Solid State Inorg Chem 33:1111-1121
Hubin R and Tarte P (1971) Etude infrarouge des orthosilicates et des orthogermanates—IV. Structures scheelite et zircon. Spectrochim Acta 27A:683-690
Hutton D, Milne B (1969) Paramagnetic resonance of Tb^{4+} in zircon. J Phys C 2:2297-2300
Hutton DR, Troup GJ (1964) Paramagnetic resonance of Gd^{3+} in zircon. Brit J Appl Phys 15:405-406
Iacconi P, Caruba R (1980) Trapping and emission centres in X-irradiated zircon (III. Influence of trivalent rare-earth impurities). Phys stat solidi (a) 62:589-596
Iacconi P, Deville A, Gaillard B (1980) Trapping and emission centres in X-irradiated zircon (II. Contribution of the SiO_4^{4-} groups). Phys stat solidi (a) 59:639-646
Ilchenko EA (1994) On hydroxyl-bearing zircons from kimberlites and kimberlite-like rocks. Mineral Zh 16:46-61 (in Russian)
Ilchenko EA, Korzhinskaya VS (1993) On hydroxyls in synthetic and natural zircons. Mineral Zh 15:26-39 (in Russian)
Ilchenko EA, Gevorkjan SV, Mitskevich BF (1988) Constitution features of zircons from the rocks of the Ukrainian shield derived from IR-spectroscopic data. Mineral Zh 10:78-83 (in Russian)
Ilchenko EA, Gevorkyjan SV, Mizkevich NYu (1989) Infrared spectroscopic characterization of zircons from rocks from the Ukrainian Shield. Mineral Zh 10:78-83 (in Russian)
Judd BR, Runciman WA (1976) Transverse Zeeman effect for ions in uniaxial crystals. Proc R Soc London 352A:91-108
Kalinichenko AM, Proshko VYa, Derskij LS, Matyash IV, Shcherbak DN, Gamarnik MYa, Ponomarenko AN (1990) On the metamictness of zircon with the aid of radiospectroscopy. Mineral Zh 12:38-43 (in Russian)
Kasuya M, Furusawa M, Ikeya M (1990) Distributions of paramagnetic centers and alpha-emitters in a zircon single crystal. Nucl Tracks Rad Meas 17:563-568
Kempe U, Götze J, Dandar S, Habermann D (1999) Magmatic and metasomatic processes during formation of the Nb-Zr-REE deposits Khaldzan Buregte and Tsakhir (Mongolian Altai): Indications from a combined CL-SEM study. Mineral Mag 63:165-177
Kempe U, Gruner T, Nasdala L, Wolf D (2000) Relevance of cathodoluminescence for the interpretation of U-Pb zircon ages, with an example of an application to a study of zircons from the Saxonian Granulite Complex, Germany. *In* Cathodoluminescence in Geosciences. Pagel M, Barbin V, Blanc P, Ohnenstetter D (eds) Springer-Verlag, Berlin–Heidelberg, p 415-455
Kempe U, Plötze M, Brachmann, A, Böttcher R (2002) Stabilisation of divalent rare earth elements in natural fluorite. Mineral Petrol 76:213-214
Kirsh Y, Townsend PD (1987) Electron and hole centers produced in zircon by X-irradiation at room temperature. J Phys C: Solid State Phys 20:967-980
Kolesov BA, Geiger CA, Armbruster T (2001) The dynamic properties of zircon studied by single-crystal X-ray diffraction and Raman spectroscopy. Eur J Mineral 13:939-948
Koschek G (1993) Origin and significance of the SEM cathodoluminescence from zircon. J Microscopy 171:223-232
Krasnobayev A, Votyakov S, Krohalev V (1988) Spectroscopy of zircons (properties and geological application). Nauka, Moscow (in Russian)
Kristanovic I (1964) X-ray investigation of zircon crystals containing OH groups. Am Mineral 49:1146-1148
Langer K (1988) UV to NIR spectra of silicate minerals obtained by microscope spectrometry and their use in mineral thermodynamics and kinetics. *In* Physical properties and thermodynamic behaviour of minerals. Salje EHK (ed) D Reidel Publishing, p 639-685
Langer K (1990) High pressure spectroscopy. *In* Absorption Spectroscopy in Mineralogy. Mottana A, Burragato F (eds) Elsevier, Amsterdam, p 228-276
Laruhin MA, van Es HJ, Bulka GR, Turkin, AA, Vainshtein, DI, den Hartog HW (2002) EPR study of radiation-induced defects in the thermoluminescence dating medium zircon ($ZrSiO_4$). J Phys: Condens Matter 14:3813-3831
Launer PJ (1952) Regularities in the infrared absorption spectra of silicate minerals. Am Mineral 37:764-784
Lazarev AN, Mirgorodskiy AP, Mazhenov NA (1980) Resonance interactions of the localized vibrators in crystals of ABO_4-type: vibration spectra of crystals with zircon and xenotime structures. *In* The Vibration of Oxide Lattices. Nauka, Leningrad, p 72-99 (in Russian)
Lehnert R., 2000. Beyond imagination—image formation based on Raman spectroscopy. GIT Imaging and Microscopy 2/2000:6-9.

Lever ABP (1968) Inorganic Electronic Spectroscopy. 1st Edn. Elsevier, Amsterdam
Lever ABP (1984) Inorganic Electronic Spectroscopy. 2nd Edn. Elsevier, Amsterdam
Long DA (1977) Raman Spectroscopy. McGraw Hill, New York, 276 p
Lork A, Koschek G (1991) Einsatz der KL-Technik bei der Beurteilung isotopengeochemisch bestimmter Alter von Zirkonen. Beitr Elektronenmikroskop Direktabb Oberfl 24:147-166
Mackey DJ, Runciman WA, Vance ER (1975) Crystal-field calculations for energy levels of U^{4+} in zirconium silicate. Phys Rev B 11:211-218
Marfunin AS (1979a) Physics of minerals and inorganic materials. Springer-Verlag, New York
Marfunin AS (1979b) Spectroscopy, luminescence and radiation centers in minerals. Springer-Verlag, Berlin
Marshall DJ (1988) Cathodoluminescence of Geological Materials. Unwin Hyman, Boston
Mazhenov NA, Murgorodskij AP, Lazarev AN (1979) Resonance-splitting of inner vibrational frequencies of heavy anions in zircon ($ZrSiO_4$) crystals. Inorg Mater 15:495-503 (in Russian)
McLaren AC, Fitz Gerald JD, Williams IS (1994) The microstructure of zircon and its influence on the age determination from Pb/U isotopic ratios measured by ion microprobe. Geochim Cosmochim Acta 58:993-1005
McMillan P (1985) Vibrational spectroscopy in the mineral science. Rev Mineral 14:9-63
Mumpton FA, Roy R (1961) Hydrothermal stability studies of the zircon-thorite group. Geochim Cosmochim Acta 21:217-238
Nasdala L (1993) Ramanspektroskopische Untersuchungen an ausgewählten Mineralen. PhD dissertation, Bergakademie, Freiberg
Nasdala L (2002) Raman mapping – a tool for revealing internal structures of minerals. Acta Universitatis Carolinae, Geologica 46:61-62.
Nasdala L, Massonne H-J (2000) Microdiamonds from the Saxonian Erzgebirge, Germany: *in situ* micro-Raman characterization. Eur J Mineral 12:495-498
Nasdala L, Irmer G, Wolf D (1995) The degree of metamictization in zircon: a Raman spectroscopic study. Eur J Mineral 7:471-478
Nasdala L, Pidgeon RT, Wolf D (1996) Heterogeneous metamictization of zircon on a microscale. Geochim Cosmochim Acta 60:1091-1097
Nasdala L, Pidgeon RT, Wolf D, Irmer G (1998a) Metamictization and U-Pb isotopic discordance in single zircons: a combined Raman microprobe and SHRIMP ion probe study. Mineral Petrol 62:1-27
Nasdala L, Götze J, Pidgeon RT, Kempe U, Seifert T (1998b) Constraining a U-Pb age: micro-scale characterization of zircons from Saxonian Rotliegend rhyolites. Contrib Mineral Petrol 132:300-306
Nasdala L, Wenzel T, Pidgeon RT, Kronz A (1999) Internal structures and dating of complex zircons from Meissen Massif monzonites, Saxony. Chem Geol 156:331-341
Nasdala L, Banerjee A, Häger T, Hofmeister W (2001a) Laser-Raman micro-spectroscopy in mineralogical research. Microsc Analysis, Eur Ed 70:7-9
Nasdala L, Beran A, Libowitzky E, Wolf D (2001b) The incorporation of hydroxyl groups and molecular water in natural zircon ($ZrSiO_4$). Am J Sci 301:831-857
Nasdala L, Wenzel M, Andrut M, Wirth R, Blaum P (2001c) The nature of radiohaloes in biotite: Experimental studies and modeling. Am Mineral 86:498-512
Nasdala L, Wenzel M, Vavra G, Irmer G, Wenzel T, Kober B (2001d): Metamictisation of natural zircon: Accumulation versus thermal annealing of radioactivity-induced damage. Contrib Mineral Petrol 141:125-144
Nasdala L, Lengauer CL, Hanchar JM, Kronz A, Wirth R, Blanc P, Kennedy AK, Seydoux-Guillaume A-M (2002a) Annealing radiation damage and the recovery of cathodoluminescence. Chem Geol 191:121-140
Nasdala L, Irmer G, Jonckheere R (2002b) Radiation damage ages: Practical concept or impractical vision? – Reply to two comments on "Metamictization of natural zircon: Accumulation versus thermal annealing of radioactivity-induced damage", and further discussion. Contrib Mineral Petrol 143:758-765
Nasdala L, Garver JI, Reiners PW, Kennedy AK, Stern RA, Balan E, Wirth R (submitted) Incomplete retention of radiation damage in zircon from Sri Lanka. Am Mineral
Nechaev SV, Krivdik SG, Krochuk VM, Mizkevich NYu, Tkachuk VI (1986) Zircons form syenites from the Yastrebezkij Massif (Ukrainian Shield)—indicators for conditions of their crystallization. Mineral Zh 8:45-56 (in Russian)
Newman DJ (1971) Theory of lanthanide crystal fields. Adv Phys 20:197-256
Newman DJ, Ng B (1989) The superposition model of crystal fields. Rep Prog Phys 52:699-763
Nicola JH, Rutt HN (1974) A comparative study of zircon ($ZrSiO_4$) and hafnon ($HfSiO_4$) Raman spectra. J Phys C: Solid State Phys 7:1381-1386
Norman CE (2002) Reaching the spatial resolution limits of SEM-based CL and EBIC. Eur Microsc Anal 76:9-12
Nuttall RHD, Weil JA (1981a) The magnetic properties of the oxygen-hole aluminium centers in crystalline SiO_2. I. $[AlO_4]^0$. Can J Phys 59:1696-1708
Nuttall RHD, Weil JA (1981b) The magnetic properties of the oxygen-hole aluminium centers in crystalline SiO_2. II. $[AlO_4/H^+]^+$ and $[AlO_4/Li^+]^+$. Can J Phys 59:1709-1718

Ohnenstetter D, Cesbron F, Remond G, Caruba R, Claude JM (1991) Emissions de cathodoluminescence de deux populations de zircons naturels: tentative d'interpretation. C R Acad Sci Paris 313:641-647

Panczer G (2001) La photoluminescence résolue en temps, nouvel outil pour la minéralogie. Habilitation thesis, Université Claude Bernard, Lyon

Pellas P (1965) Étude sur la recristallisation thermique des zircons métamictes. Mémoires du Museum National d'Histoire Naturelle, Sér C, Sciences de la Terre, 12:227-253

Phillips MR, Kalceff MAS, Moon AR (1996) Cathodoluminescence spectroscopy of natural zircon (abstr). *In* Intl Conf on Cathodoluminescence and Related Techniques in Geosciences and Geomaterials. Pagel M (ed) Nancy, p 115-116

Pidgeon RT (1992) Recrystallization of oscillatory zoned zircon: some geochronological and petrological implications. Contrib Mineral Petrol 110:463-472

Pidgeon RT, O'Neill J, Silver LT (1966) Uranium and lead isotopic stability in a metamict zircon under experimental hydrothermal conditions. Science 154:1538-1540

Pidgeon RT, O'Neill J, Silver LT (1973) Observations on the crystallinity and the U-Pb isotopic system of a metamict Ceylon zircon under experimental hydrothermal conditions. Fortschr Mineral 50:118

Pidgeon RT, Nasdala L, Todt W (1998) Determination of radiation damage ages on parts of zircon grains by Raman microprobe: implications for annealing history and U-Pb stability. Mineral Mag 62A:1174-1175

Pointer CM, Ashworth JR, Ixer RA (1988) The zircon-thorite mineral group in metasomatized granite, Ririwai, Nigeria. 2. Zoning, alteration and exsolution in zircon. Mineral Petrol 39:21-37

Poirot I, Kot W, Shalimoff G, Edelstein N, Abraham MM, Finch CB, Boatner LA (1988) Optical and EPR investigations of Np^{4+} in single crystals of $ZrSiO_4$. Phys Rev B: Condens Matter 37:3255-3264

Poirot IS, Kot WK, Edelstein NM, Abraham MM, Finch CB, Boatner LA (1989) Optical study and analysis of Pu^{4+} in single crystals of $ZrSiO_4$. Phys Rev B: Condens Matter 39:6388-94

Poller U (2000) A combination of single zircon dating by TIMS and cathodoluminescence investigations on the same grain: the CLC method—U-Pb geochronology for metamorphic rocks. *In* Cathodoluminescence in Geosciences. Pagel M, Barbin V, Blanc P, Ohnenstetter D (eds) Springer, Berlin–Heidelberg, p 401-414

Poller U, Huth J, Hoppe P (2000) SEE und U-Th-Pb Ionensondenmikroanalysen an Zirkonen zum Verständnis von Kathodolumineszenzsignalen. Eur J Mineral 12:155

Poller U, Huth J, Hoppe P, Williams IS (2001) REE, U, Th, and Hf distribution in zircon from Western Carpathian Variscan granitoids: a combined cathodoluminescence and ion microprobe study. Am J Sci 301:858-876

Povarennych AS, Melnik YuP, Shabalin BG (1977) On synthesis and IR-spectra of zircon and hafnon. Geol Zh 37:131-135 (in Russian)

Rakovich FI, Gevorkyan SV (1988) Zircons, associated with uranium minerals. Mineral sbornik 42:65-68 (in Russian)

Reiners PW, Farley KA, Hickes HJ (2002) He diffusion and (U-Th)/He thermochronometry of zircon: Initial results from Fish Canyon Tuff and Gold Butte, Nevada. Tectonophysics 349:297-308

Remond G, Cesbron F, Chapoulie R, Ohnenstetter D, Roques-Carmes C, Schvoerer M (1992) Cathodoluminescence applied to the microcharacterization of mineral materials: a present status in experimentation and interpretation. Scanning Microsc Intl 6:23-68

Remond G, Phillips MR, Roques-Carmes C (2000) Importance of instrumental and experimental factors on the interpretation of cathodoluminescence data from wide band gap materials. *In* Cathodoluminescence in Geosciences. Pagel M, Barbin V, Blanc P, Ohnenstetter D (eds) Springer, Berlin–Heidelberg, p 59-126

Richman I, Kisliuk P, Wong EY (1967) Absorption spectrum of U^{4+} in zircon ($ZrSiO_4$). Phys Rev 155:262-267

Ríos S, Salje EKH, Zhang M, Ewing RC (2000) Amorphization in zircon: evidence for direct impact damage. J Phys: Condens Matter 12:2401-2412

Robinson K, Gibbs GV, Ribbe PH (1971) The structure of zircon: a comparison with garnet. Am Mineral 56:782-790

Roger F, Calassou S, Lancelot J, Malavieille J, Mattauer M, Zhiqin Xu, Ziwen H, Liwei H (1995) Miocene emplacement and deformation of the Koga Shan granite (Xianshui He fault zone, west Sichuan, China): geodynamic implications. Earth Planet Sci Lett 130:201-216

Romans PA, Brown LL, White JC (1975) An electron microprobe study of yttrium, rare earth, and phosphorus distribution in zoned and ordinary zircon. Am Mineral 60:475-480

Rossman GR (1988) Optical spectroscopy. Rev Mineral 18:207-254

Rubatto D, Gebauer D (2000) Use of cathodoluminescence for U-Pb zircon dating by ion microprobe: some examples from the Western Alps. *In* Cathodoluminescence in Geosciences. Pagel M, Barbin V, Blanc P, Ohnenstetter D (eds) Springer, Berlin–Heidelberg, p 373-400

Rubin JN, Henry CD, Price JG (1989) Hydrothermal zircons and zircon overgrowths, Sierra Blance Peaks, Texas. Am Mineral 74:865-869

Rudnitskaya ES, Lipova E (1972) Infrared spectroscopic and nuclear magnetic resonance study of metamict zircon. Geologiya i Razvedka 4:43-50 (in Russian)

Saksena VD (1961) Infrared absorption studies of some silicate structures. Trans Faraday Soc 57:242

Salje EKH, Chrosch, J, Ewing RC (1999) Is "metamictization" of zircon a phase transition? Am Mineral 84:1107-1116

Samoylovich MI, Novozhilov AI, Barsanov GP (1968) Electron paramagnetic resonance in irradiated zircons containing vicarious elements. Geokhimiya 1968:494-495 (in Russian)
Schläfer HL, Gliemann G (1980) Einführung in die Ligandenfeldtheorie. Akademische Verlagsgesellschaft, Frankfurt/Main
Shinno I (1986) Three types of photo-luminescence in natural zircon. J Japan Assoc Mineral Petrol Econ Geol 81:433-445
Shinno I (1987) Color and photo-luminescence of rare-earth element doped zircon. Mineral J 13/5:239-253
Solntsev VP, Shcherbakova MYa (1972) Electron paramagnetic resonance of Ti^{3+} in alpha-quartz and zircon. Zh Strukt Khim 13:924-927 (in Russian)
Solntsev VI, Shcherbakova MYa (1973) A study of lattice defects in irradiated zircon by the EPR method. Doklady Akademii Nauk SSSR 212:156-158 (in Russian)
Solntsev VP, Shcherbakova MYa (1974) Charge compensation mechanisms and the form in which Nb and Y are incorporated into the structure of zircon. Inorg Mater 10:1574-1577
Solntsev VP, Shcherbakova Mya, Dvornikov EV (1974) SiO_2^-, SiO_3^{3-}, and SiO_4^{5-} radicals in the $ZrSiO_4$ structure from electron paramagnetic resonance data. Zh strukt khim 15:217-221 (in Russian; English abstr: J Struct Chem 15:201-204)
Sommerauer J (1976) Die chemisch-physikalische Stabilität natürlicher Zirkone und ihr U-(Th)-Pb System. PhD dissertation, Eidgenössische Technische Hochschule, Zürich
Speer JA (1980) Zircon. Rev Mineral 5:67-103
Syme RWG, Lockwood DJ, Kerr J (1977) Raman spectrum of synthetic zircon ($ZrSiO_4$) and thorite ($ThSiO_4$). J Phys C: Solid State Phys 10:1335-1348
Taran MN, Bagmut NN, Kislyakova TY, Kvasnitsa VN (1990a) Spectral characteristics of zircon from mantle-derived rocks and its prospecting significance. Mineral Sbornik 44:60-64 (in Russian)
Taran MN, Bagmut NN, Kvasnytsya VN, Kharkiv AD (1990b) Optical and ESR spectra of natural zircons of kimberlitic type. Mineral Zh 12:44-51 (in Russian)
Tarashchan A (1978) Luminescence of Minerals. Naukova Dumka, Kiev, 296 p (in Russian)
Tartaj P, Sanz J, Serna CJ and Ocana M 1994 Zircon formation from amorphous spherical $ZrSiO_4$ particles obtained by hydrolyses of aerosols. J Mater Sci 29:6533-6538
Tennant WC, Claridge RFC (1999) Large-magnitude high-spin nuclear parameters in a Ti^{3+} center from X-band EPR measurements at 10 K. J Magn Reson 137:122-131
Townsend PD, Rowlands AP (2000) Information encoded in cathodoluminescece emission spectra. *In* Cathodoluminescence in Geosciences. Pagel M, Barbin V, Blanc P, Ohnenstetter D (eds), Springer, Berlin–Heidelberg, p 41-57
Trinkler M, Kempe U, Plötze M, Rieser U (1993) Über rosa und braunen Fluorit aus Sn-W-Lagerstätten. Chem Erde 53:165-181
Valéro R, Delmotte L, Louis J, Durand B, Guth JL and Chopin T (1999) A new hydrothermal fluoro-zircon. J Mater Chem 9:117-123
Vance ER (1974) The anomalous optical absorption spectrum of low zircon. Mineral Mag 39:709-714
Vance ER (1975) α-recoil damage in zircon. Radiat Eff 24:1-6
Vance ER, Anderson BW (1972a) Study of metamict Ceylon zircon. Mineral Mag 38:605-613
Vance ER, Anderson BW (1972b) Differences among low Ceylon zircons. Mineral Mag 38:721-724
Vance ER, Mackey DJ (1974) Optical study of U^{5+} in zircon. J Phys C: Solid State Phys 7:1898-1909
Vance ER, Mackey DJ (1975) Further studies of the optical absorption spectrum of U^{5+} in zircon. J Phys C: Solid State Phys 8:3439-3447
Vance ER, Mackey DJ (1978) Optical spectra of U^{4+} and U^{5+} in zircon, hafnon, and thorite. Phys Rev B 18:185-189
Valishev RM, Vinokurov VM, Zaripov MM, Stepanov VG (1965) Electron paramagnetic resonance of the Er^{3+} ions in zircon $ZrSiO_4$ crystals. Geokhimiya 1965:1265 (in Russian)
Vavra G (1990) On the kinematics of zircon growth and its petrogenetic significance: a cathodo-luminescence study. Contrib Mineral Petrol 106:90-99
Vavra G (1994) Systematics of internal zircon morphology in major Variscan granitoid types. Contrib Mineral Petrol 117:331-344
Vavra G, Gebauer D, Schmid R, Compston W (1996) Multiple zircon growth and recrystallization during polyphase Late Carboniferous to Triassic metamorphism in granulites of the Ivrea Zone (Southern Alps): an ion microprobe (SHRIMP) study. Contrib Mineral Petrol 122:337-358
Vavra G, Schmid R, Gebauer D (1999) Internal morphology, habit and U-Th-Pb microanalysis of amphibolite-to-granulite facies zircons: geochronology of the Ivrea Zone (Southern Alps). Contrib Mineral Petrol 134:380-404
Veytizou C, Quinson JF and Douy A (2000) Sol-gel synthesis via aqueous semi-alkoxide route and characterization of zircon powder. J Mater Chem 10:365-370
Vinokurov VM, Gainullina NM, Evgrafova LA, Nizamutdinov NM, Suslina AN (1971) $Zr^{4+} \rightarrow Y^{3+}$ isomorphism in zircon and the associated charge compensation. Kristallografiya 16:318-323 (in Russian; English abstr: Sov Phys

Crystallogr 16:262-265)
Vinokurov VM, Gainullina NM, Nizamutdinov NM, Krasnobayev AA (1972) Distribution of admixed Fe^{3+} ions in the single zircon crystals from the kimberlite pipe "Mir." Geokhimiya 1972:1402-1405 (in Russian; English translation: Geochim Intl 9:952-954)
Vinokurov VM, Zaripov MM, Polskiy YuE, Stepanov VG, Chirkin GK, Shekun LYa (1963) Radiospectroscopic detection of small amounts of Eu^{2+}, Gd^{3+} and Nb^{4+} and their isomorphism in fluorite and zircon. Geokhimiya 1963:1002-1007 (in Russian)
Votyakov SL, Ivanov IP, Krasnobayev AA, Krokhalev VY, Korzhinskaya VS (1986) Spectroscopic-luminescent properties of zircon orthosilicate grown by the hydrothermal method. Neorganicheskie materialy 22:281-286 (in Russian)
Votyakov SL, Krasnobayev AA, Krokhalev VY (1993) The Problems of Applied Spectroscopy of Minerals. Nauka, Ekaterinburg, 233 p (in Russian)
Walsby CJ, Lees NS, Tennant WC, Claridge RFC (2000) 15 K EPR of an oxygen-hole boron center, $[BO_4]^0$, in x-irradiated zircon. J Phys: Condens Matter 12:1441-1450
Wasilewski PJ, Senftle FE, Vaz JE, Thorpe AN, Alexander CC (1973) A study of the natural a-recoil damage in zircon by infrared spectra. Radiat Eff 17:191-199
Wertz JE, Bolton JR (1972) Electron spin resonance elementary theory and practical applications. McGraw-Hill, New York
Whitehouse MJ, Kamber BS, Moorbath S (1999) Age significance of U-Th-Pb zircon data from early Archean rocks of west Greenland - a reassessment based on combined ion-microprobe and imaging studies. Chem Geol 160:201-224
Wiedenbeck M, Allé P, Corfu F, Griffin WL, Meier M, Oberli F, von Quadt A, Roddick JC, Spiegel W (1995) Three natural zircon standards for U-Th-Pb, Lu-Hf, trace element and REE analysis. Geostandards Newsletter 19(1):1-23
Woodhead JA, Rossman GR, Silver LT (1991a) The metamictization of zircon: radiation dose-dependent structural characteristics. Am Mineral 76:74-82
Woodhead JA, Rossman GR, Thomas AP (1991b) Hydrous species in zircon. Am Mineral 76:1533-1546
Wopenka B, Jolliff BL, Zinner E, Kremser DT (1996) Trace element zoning and incipient metamictization in a lunar zircon: application of three microprobe techniques. Am Mineral 81:902-912
Yang B, Luff BJ, Townsend PD (1992) Cathodoluminescence of natural zircons. J Phys: Condens Matter 4:5617-5624
Yang XM, Zhang PS, Zhan WL (1990) Infrared-spectra effect of alpha-decay damage in zircon structure. Chinese Sci Bull 35:1988-1991
Zhang M, Salje EKH (2001) Infrared spectroscopic analysis of zircon: Radiation damage and the metamict state. J Phys: Condens Matter 13: 3057-3071
Zhang M, Salje EKH (2003) Spectroscopic characterization of metamictization and recrystallization in zircon and titanite. Phase Transitions 76:117-136
Zhang M, Salje EKH, Farnan I, Graeme-Barber A, Daniel P, Ewing RC, Clark AM, Lennox H (2000a) Metamictization of zircon: Raman spectroscopic study. J Phys: Condens Matter 12:1915-1925
Zhang M, Salje EKH, Capitani GC, Leroux H, Clark AM, Schlüter J, Ewing RC (2000b) Annealing of a-decay damage in zircon: a Raman spectroscopic study. J Phys: Condens Matter 12:3131-3148
Zhang M, Salje EKH, Ewing RC, Farnan I, Ríos S, Schlüter J, Leggo P (2000c) α-decay damage and recrystallization in zircon: Evidence for an intermediate state from infrared spectroscopy. J Phys: Condens Matter 12:5189-5199
Zhang M, Salje EKH, Ewing RC (2002) IR Spectra of Si-O overtones, hydrous species and U ions in metamict zircon: Radiation damage and recrystallization. J Phys: Condens Matter 14:3333-3352
Zhang M, Salje EKH, Ewing RC (submitted) Oxidation state of uranium in metamict and annealed zircon: Near infrared spectroscopic quantitative analysis. EUG, Nice